SEEING TO GENERALIZE: HOW VISUAL DATA CORRECTS BINDING SHORTCUTS

Nicolas Buzeta[*1,2], **Felipe del Rio**[1,2], **Cristian Hinostroza**[1,2],
Denis Parra[1,2,3], **Hans Lobel**[1,2] **& Rodrigo Toro Icarte**[1,2]
[1]Department of Computer Science, Pontificia Universidad Católica, Santiago, Chile
[2]Centro Nacional de Inteligencia Artificial (CENIA), Santiago, Chile
[3]Instituto Milenio en Ingeniería e Inteligencia Artificial para la Salud (iHEALTH), Santiago, Chile
nicolas.buzeta@uc.cl

ABSTRACT

Vision Language Models (VLMs) are designed to extend Large Language Models (LLMs) with visual capabilities, yet in this work we observe a surprising phenomenon: VLMs can outperform their underlying LLMs on purely text-only tasks, particularly in long-context information retrieval. To investigate this effect, we build a controlled synthetic retrieval task and find that a transformer trained only on text achieves perfect in-distribution accuracy but fails to generalize out of distribution, while subsequent training on an image-tokenized version of the same task nearly doubles text-only OOD performance. Mechanistic interpretability reveals that visual training changes the model's internal binding strategy: text-only training encourages positional shortcuts, whereas image-based training disrupts them through spatial translation invariance, forcing the model to adopt a more robust symbolic binding mechanism that persists even after text-only examples are reintroduced. We further characterize how binding strategies vary across training regimes, visual encoders, and initializations, and show that analogous shifts occur during pretrained LLM-to-VLM transitions. Our findings suggest that cross-modal training can enhance reasoning and generalization even for tasks grounded in a single modality.

1 INTRODUCTION

Large Language Models (LLMs) excel at a wide range of text-based tasks, from summarization to mathematical reasoning Devlin et al. (2019); Brown et al. (2020); Wei et al. (2022); Ahn et al. (2024); Zhang et al. (2024b). However, on their own, they cannot leverage visual information. Vision–Language Models (VLMs) address this limitation by learning to encode images into token representations that a pre-trained LLM can consume to perform vision-centric tasks such as image captioning and visual question answering Alayrac et al. (2022); Zhang et al. (2024a). A standard training pipeline begins by taking a pre-trained LLM and augmenting it with a vision encoder—typically a vision transformer Dosovitskiy et al. (2021)—that maps visual inputs into a sequence of tokens Li et al. (2023). These visual tokens are then fed into the LLM, and the combined system is trained end-to-end on tasks that require both visual and textual understanding Bai et al. (2023); Liu et al. (2023).

In this paper, we study an intriguing observation: in some cases, VLMs outperform their underlying pre-trained LLMs on text-only tasks. That is, for certain tasks that require exclusively textual reasoning, the performance of the original LLM improves after being further trained on objectives that consider vision and language elements. We find that this scheme significantly and systematically enhances performance on information retrieval problems Liu et al. (2024); Feng & Steinhardt (2024); Gur-Arieh et al. (2025); Urrutia et al. (2025), especially in long-context settings. For instance, in our experiments, the VLM Qwen3-VL-8B Yang et al. (2025a) achieves 76.0% accuracy on a text-only retrieval task, while its base model Qwen3-8B reaches only 62.6% on the same evaluation. This

[*]Equal contribution.

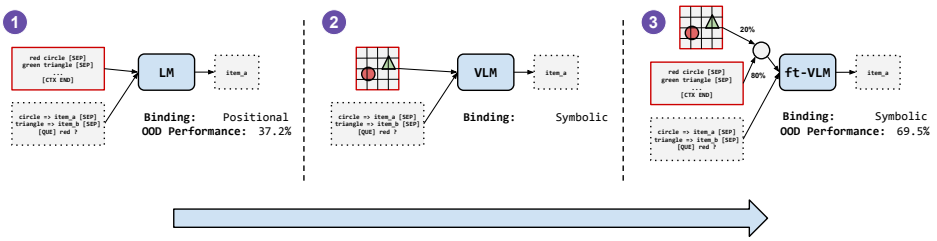

Figure 1: Overview of the training pipeline, showing the progression from text-only training to vision–language training.

result is puzzling: why would training on image-based tasks lead to systematic improvements on purely text-based evaluations?

To study this question, we designed a set of controlled experiments centered on a text-only retrieval task (shown in Figure 1). At a high level, the task involves describing a set of colored shapes, assigning a letter to each shape, and querying the model for the letter associated with a shape of a specified color. For example, given the context description "*red circle and green triangle*" and the associations "*the circle is item_a and the triangle is item_b,*" the model is asked "*which item corresponds to the red shape*" (the correct answer being *item_a*). We trained a small transformer model to solve this task using contexts containing up to eight shapes (first row in Figure 1). The model quickly mastered the task, achieving perfect in-distribution accuracy—i.e., when the input contained at most eight objects. However, its out-of-distribution (OOD) generalization was poor: on contexts with more than eight shapes, its accuracy dropped to 37.2%.

We then continued training the same transformer on an equivalent retrieval task, replacing the textual context descriptions with tokenized images of the shapes and their colors (second and third rows in Figure 1). Training initially relied exclusively on image-based contexts, and we later introduced a mixture of image-only and text-only instances. Crucially, throughout all stages of training, the model was exposed only to contexts containing at most eight objects. After this additional training, the model exhibited the same puzzling phenomenon observed in pre-trained models: the vision-language model showed a substantial OOD performance improvement over the base model on the original text-only retrieval task, rising from 37.2% to 69.5%.

Having replicated the phenomenon in a controlled setting, we use mechanistic interpretability to examine how visual training alters the language model's internal computations. We find that visual training fundamentally changes the model's binding strategy—the mechanism by which it links information across tokens. Prior work has shown that LLMs employ different binding mechanisms to solve in-context reasoning problems (e.g., Gur-Arieh et al., 2025; Urrutia et al., 2025). In particular, positional binding relies on token positions within the sequence, whereas symbolic binding uses the semantic content of tokens to establish associations. Following the methodology of Gur-Arieh et al. (2025), we find that a model trained only on text almost exclusively relies on positional binding. In our retrieval task, this manifests as a shortcut Geirhos et al. (2020): the model exploits positional regularities in contexts containing up to 8 shapes, instead of attending to semantic content.

However, once the model is further trained on image-based versions of the task, positional binding becomes ineffective. Unlike sequences, images lack a canonical ordering, and visual models are typically designed to be robust to spatial translations. Consequently, spatial layouts do not reliably correspond to token ordering, rendering position-based shortcuts unreliable. As a result, the model shifts its internal strategy and begins relying predominantly on symbolic binding. Remarkably, when we subsequently reintroduce text-only examples, the model continues to use this new, more robust symbolic binding strategy to solve the original task. This shift in binding behavior explains the improved OOD performance: symbolic binding is inherently better suited for information retrieval, particularly in settings involving long or variable-length contexts.

We explore how binding strategies vary across training regimes and show that image training consistently promotes symbolic binding. We demonstrate that these gains are not explained by indirect exposure to longer contexts, and that similar shifts occur in pretrained VLMs. These observa-

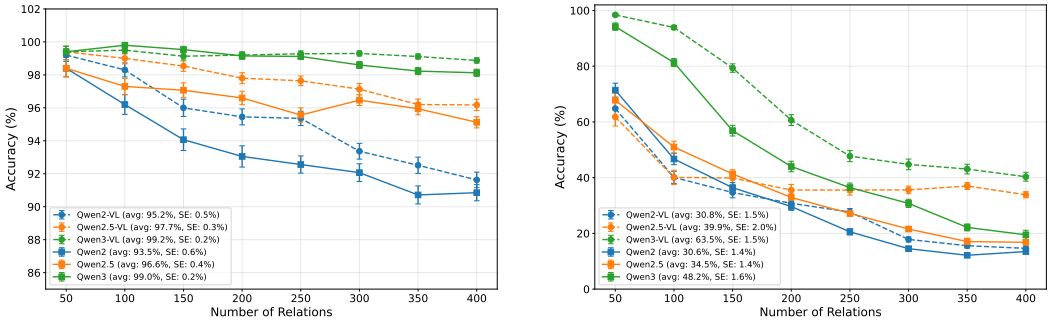

(a) Direct Retrieval

(b) Indirect Retrieval

Figure 2: Binding accuracy comparison between text-only LLMs and their VLM counterparts across three model generations. VLMs consistently outperform LLMs as context length increases. The left panel shows performance on the simpler direct retrieval task, while the right panel shows the harder indirect retrieval task. Individual breakdown per model is provided in Appendix A.

tions raise broader questions about how multimodal curricula shape internal representations—and whether similar effects might emerge from other modalities or data augmentations.

2 VLM Gains on Text-Only Tasks

We first show that VLMs outperform their base LLM on text-only tasks that require retrieving information from long contexts. To study this effect, we focus on the Qwen family of models, since both their Instruct and VL-Instruct variants are publicly available across multiple generations. In particular, we evaluate versions 2 Yang et al. (2024), 2.5 Yang et al. (2025b), and 3 Yang et al. (2025a) as released, without any task-specific fine-tuning or post-processing (see Appendix B for details on the evaluation setup).

To evaluate retrieval abilities, we employ two synthetic tasks: *Direct Retrieval* and *Indirect Retrieval*. In the Direct Retrieval task, the objective is to determine where a person lives given a large textual context. Formally, let $\mathcal{N}$ denote a set of names and C a set of cities. Each input consists of a context containing l statements of the form "n_i lives in c_i," where each $n_i \in \mathcal{N}$ and each $c_i \in C$ appears exactly once within the context. The query then asks for the city associated with one of the names mentioned in the context. For example (with the model's output highlighted in blue):

> **Context:** James lives in Tokyo. Mary lives in Paris. John lives in Mumbai. **Question:** In what city does John live? John lives in Mumbai

The Indirect Retrieval task introduces an additional reasoning step. In addition to $\mathcal{N}$ and C, we define a set of foods $\mathcal{F}$. The context is divided into two parts. The first contains statements of the same form as in the Direct Retrieval task, "n_i lives in c_i". The second contains l statements of the form "f_i is liked by n_i." Each name n_i appears exactly once in each part, so the index i links a food f_i to a city c_i through the same person n_i. The query refers to a food rather than a name, requiring the model to first identify the corresponding person and then retrieve their city. For instance, a concrete example with three pairs (with the model's output highlighted in blue) would be:

> **Context:** Banana is liked by Mary. Orange is liked by John. Mary lives in Paris. John lives in Mumbai. **Question:** Where does the person that likes Orange live? Answer with just the city name. **City:** Mumbai

Both tasks are inspired by the *Capitals* task of Feng & Steinhardt (2024). Direct Retrieval task tests basic context lookup, while Indirect Retrieval task adds a compositional retrieval step. Importantly, neither task requires prior world knowledge (e.g., real-world capitals), since all necessary information is contained within the provided context.

Figure 2 presents the results for both the Direct and Indirect Retrieval tasks across several models from the Qwen family. For each context length l, we generated 10 independent contexts. Each model was evaluated on every query position within each context, resulting in a total of $10 \times l$ queries for

that length. We report the mean accuracy and standard error for each model across all evaluated context lengths.

In the Direct Retrieval task, VLMs consistently outperform their LLM counterparts across nearly all context lengths, with Qwen3-VL models achieving near-ceiling accuracies of approximately 98% even at $l = 400$. This performance gap becomes even more pronounced in the Indirect Retrieval task, where VLMs demonstrate a clear and persistent advantage over their corresponding base LLMs. This outcome is particularly surprising given that VLMs are trained primarily to enable LLMs to interpret visual information. Why, then, do VLMs also exhibit consistently superior performance on purely text-based retrieval tasks?

In the following section, we aim to reproduce this phenomenon in a controlled setting, which will allow us to investigate it using mechanistic interpretability tools.

3 Problem Formulation

To isolate the role of modality in the performance gap between VLMs and LLMs, we introduce a modified Indirect Retrieval task that enables controlled switching between modalities while keeping the underlying task unchanged.

The task links colored shapes and unique target labels. The model must first track objects defined by both their shape and color (e.g., a red triangle). It is then presented with a separate list of associations (e.g., "the triangle is item a"). The challenge is to retrieve the correct target item when queried using only the object's color (e.g., returning item a when asked about "red"), as illustrated in the first step of Figure 1. Using simple visual primitives such as shapes and colors allows the task can be presented identically across modalities—either as a textual description or as an image—without altering its underlying structure (see Figure 1).

We now formally define our Indirect Retrieval task. Let $\mathcal{A}$ be a set of attributes (e.g., colors), $\mathcal{E}$ a set of entities (e.g., shapes), and $\mathcal{I}$ a set of items (e.g., `item001`). The goal is to map a query attribute $q \in \mathcal{A}$ to a target item $y \in \mathcal{I}$ through an intermediate entity $e \in \mathcal{E}$. Solving the task requires two reasoning steps. First, the model must identify the entity e associated with the query attribute q using the context set $\mathcal{C} = (a_i, e_i)_i$, where $a_i \in \mathcal{A}$ and $e_i \in \mathcal{E}$. Second, it must retrieve the item y linked to that entity using the association set $\mathcal{B} = (e_j, y_j)_j$, where $e_j \in \mathcal{E}$ and $y_j \in \mathcal{I}$. We consider two instantiations of this task: one presented entirely in text and another that combines images with text.

The unified prompt structure for both modalities is:

$$\mathbf{x} = [\mathbf{X}_{\text{context}}, \texttt{[CTX_END]}, \mathbf{X}_{\text{associations}}, \texttt{[QUE]}, \mathbf{x}_{\text{query}}]$$

where $\mathbf{X}_{\text{associations}}$ is a sequence of text tokens defining the Entity $\rightarrow$ Item assignments (e.g., `shape01`$\rightarrow$`item01`), while `[CTX_END]` and `[QUE]` are special delimiter tokens. Then, for both tasks, we define the context $\mathbf{X}_{\text{context}}$ as a sequence of attribute-entity pairs (a_i, e_i).

In the **text modality**, the context is represented as follows:

$$\mathbf{X}^{\text{text}}_{\text{context}} = [a_1, e_1, a_2, e_2, \ldots, a_N, e_N]$$

where each pair is described sequentially (e.g., "red square"). In the **vision modality**, the context is a sequence of images where each entity e_i is rendered with attribute a_i:

$$\mathbf{X}^{\text{image}}_{\text{context}} = [\texttt{<IMG>}_1, \texttt{<IMG>}_2, \ldots, \texttt{<IMG>}_N]$$

4 VLM Gains in a Controlled Setting

In this section, we replicate the performance gains of VLMs over LLMs reported in Section 2 by training a 12-layer decoder-only Transformer on the Indirect Retrieval task. To accomplish this, we first train the model exclusively on the text modality, where the context $\mathbf{X}^{\text{text}}_{\text{context}}$ consists of sequential token pairs representing attribute–entity associations (e.g., "red triangle", "blue circle"). Training proceeds until contexts contain up to 8 objects and validation performance saturates, resulting in the baseline text-only model $\mathcal{M}_{\text{text-only}}$ (see Appendix D for further details).

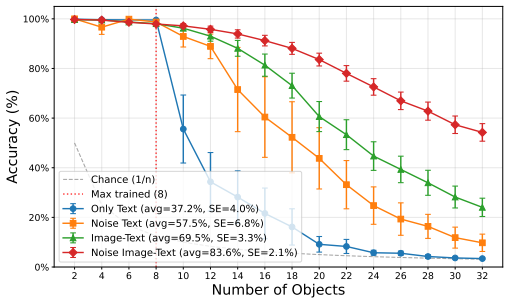

Figure 3: **Generalization performance.** Text-Only (37.2%), Image-Text (69.5%), Noise-Text (57.5%), N-I-T (83.6%).

Model	Peak Layer	Sym./Pos. Ratio	Δ
Qwen 2	22	1.383	—
Qwen 2-VL	22	1.499	+0.116
Qwen 2.5	22	1.218	—
Qwen 2.5-VL	22	1.282	+0.064
Qwen 3	28	1.819	—
Qwen 3-VL	28	2.463	+0.644

Table 1: **Binding Mechanisms.** Ratio of symbolic to positional mechanism attribution.

Next, we continue training the same model exclusively on the image modality. As described in Section 3, the Indirect Retrieval task can be instantiated in both text and vision modalities. In the vision setting, the context $\mathbf{X}_{\text{context}}^{\text{image}}$ consists of rendered images in which each entity is depicted with its associated attribute (e.g., colored shapes, see Appendix C for further details). To study the impact of visual training, we replace the text context with token representations extracted from a frozen, pretrained image encoder. We experiment with three encoder architectures: a supervised CNN-based ResNet-152 He et al. (2016), a supervised Transformer-based ViT-B/16 Dosovitskiy et al. (2021), and a self-supervised Transformer-based DINOv3 Siméoni et al. (2025). Each variant is trained until validation performance saturates.

Finally, we transfer the model back to the text domain while keeping the restricted parameter set (8 colors, 13 shapes, 8 items) and train on a mixed curriculum comprising 20% image-based and 80% text-based tasks. For OOD evaluation, we expand the training distribution to match the full complexity of the baseline text model (216 colors, 216 shapes, 32 items), yielding the final model $\mathcal{M}_{\text{image-text}}$.

Figure 3 compares the two models on the Indirect Retrieval task in the text modality as the number of objects in the context increases. We train $\mathcal{M}_{\text{text-only}}$ with four random seeds. From each, we initialize and train separate image-modality variants using three image encoders (ResNet-152, ViT, and DINOv3), resulting in a total of 12 runs for $\mathcal{M}_{\text{image-text}}$.

As the figure shows, the text-only model, $\mathcal{M}_{\text{text-only}}$ (blue curve), generalizes poorly to OOD sequence lengths: its accuracy drops sharply beyond the training maximum of eight items, yielding an average OOD accuracy of 37.2%. In contrast, $\mathcal{M}_{\text{image-text}}$ (green curve) shows substantially stronger generalization, achieving an average OOD accuracy of 69.5%. This large improvement demonstrates that training on visual inputs enhances generalization in the text modality, mirroring the phenomenon observed in large-scale VLMs.

Noise Augmentation. One possible hypothesis about why $\mathcal{M}_{\text{image-text}}$ outperforms $\mathcal{M}_{\text{text-only}}$ is that the improvement arises from exposure to longer sequences during visual training. Image encoders produce sequences of patch tokens (e.g., 196 tokens for a 14×14 grid), meaning the model encounters a broader range of positional indices than in text-only training, where contexts contain at most 8 object pairs.

To test whether exposure to longer contexts alone explains the performance gap, we fine-tune both $\mathcal{M}_{\text{text-only}}$ and $\mathcal{M}_{\text{image-text}}$ with unattendable noise tokens Shen et al. (2023) inserted between context pairs. We denote the resulting models as $\mathcal{M}_{\text{noise-text}}$ and $\mathcal{M}_{\text{noise-image-text}}$, respectively.

The results in Figure 3 show that adding noise tokens does improve the OOD performance of the text-only model, but this effect is insufficient to account for the full gains observed with visual training. Instead, the visual modality appears to provide an additional form of regularization beyond what is achievable through simple context-length expansion.

5 EXPLAINING THE GAINS: IMAGE TRAINING INDUCES BINDING STRATEGY SHIFTS

The previous section established that visual training substantially improves OOD generalization beyond what can be explained by increased exposure to longer positional ranges. In this section, we show that the transition from $\mathcal{M}_{\text{text-only}}$ to $\mathcal{M}_{\text{image-text}}$ corresponds to a shift in how the model binds and retrieves information. Specifically, the dominant binding strategy moves from a brittle, position-dependent mechanism to a more robust, symbolic one.

We first demonstrate this shift in the clean setting, without noise augmentation. We then show that noise injection induces an intermediate mixed binding strategy in the text-only model. Finally, we connect these controlled findings to large pretrained models, showing that VLMs also rely more heavily on symbolic binding than their LLM counterparts.

5.1 BACKGROUND: BINDING MECHANISMS IN TRANSFORMERS

Recent work has identified multiple mechanisms that transformer models use for variable binding. Gur-Arieh et al. (2025) describe three main strategies. In the **positional** mechanism, the model retrieves an entity based on its ordinal position in the sequence (e.g., "the second entity"), relying heavily on positional encodings and making it sensitive to sequence structure. In the **symbolic mechanism**, retrieval is content-based: the query acts as a key that matches the associated entity in a position-agnostic way. This mechanism is referred to as *lexical* in Gur-Arieh et al. (2025) and *symbolic* in prior work on variable binding Wu et al. (2025); we adopt the term **symbolic** because it extends naturally to visual inputs, where "lexical" matching is less well-defined. Finally, the **reflexive** mechanism relies on pointer-like references and is needed when the target appears earlier than the query, preventing direct attention from query to target.

In our task, the attribute (query) consistently precedes the entity (target), making symbolic binding viable and reducing the importance of the reflexive mechanism. We therefore focus our analysis on the competition between positional and symbolic strategies.

5.2 METHODOLOGY: IDENTIFYING BINDING MECHANISMS

To determine which binding mechanism our models rely on, we use the interchange intervention proposed by Gur-Arieh et al. (2025). This method enables causal identification of binding strategies by constructing paired inputs—an original example and a counterfactual—designed so that different mechanisms would produce different predictions.

The key idea is to create input pairs where a **positional** strategy would retrieve the entity solely based on its position in the sequence, which changes between the original and counterfactual, while a **symbolic** strategy would instead retrieve the entity associated with the query's semantic content, which may remain unchanged across the pair. By patching activations from the counterfactual run into the original run at different layers, we can measure which mechanism dominates the model's computation. Full methodological details are provided in Appendix F.

5.3 THE CLEAN CASE: A COMPLETE MECHANISM SHIFT

We begin by analyzing the binding mechanisms without noise augmentation and observe a clear dichotomy between the text-only and image-trained models. Figure 4 reports, for each layer, the proportion of times the model's binding mechanism is classified as positional, symbolic, reflexive, or mixed when solving text-modality inputs containing up to eight objects. The results show that the dominant binding mechanism remains largely consistent across layers, except for the final layer. In this last layer, $\mathcal{M}_{\text{text-only}}$ adopts an almost exclusively positional strategy, meaning it heavily relies on token positions to produce the correct answer. In contrast, $\mathcal{M}_{\text{image-text}}$ primarily uses a symbolic binding mechanism, matching semantic content directly rather than depending on positional indices.

A symbolic mechanism naturally generalizes to longer contexts: because retrieval is based on semantic matching, the strategy remains valid regardless of sequence length. Positional binding, however, relies on counting or locating "the i-th binding" within the sequence, which tends to break when the model is asked to retrieve items in contexts longer than those seen during training. This

distinction explains why $\mathcal{M}_{\text{image-text}}$ generalizes better than $\mathcal{M}_{\text{text-only}}$ in the OOD evaluation presented in Section 4.

5.4 Why Images Induce the Mechanism Shift

A key difference between the two modalities is **translation invariance**, which is intrinsic to models trained on visual inputs but absent from sequential text. We hypothesize that this property plays a central role in driving the shift in binding strategy.

In the text modality, object pairs appear at specific, fixed positions in the sequence. A model can exploit this structure by learning to associate positions rather than content. This positional shortcut is highly effective within the training distribution, requiring less computational overhead than content-addressable retrieval.

In the image modality, however, the spatial position of shapes within the rendered image is essentially arbitrary. The same attribute-entity pair (e.g., a red circle) can appear at any location in the image, and this location carries no task-relevant information. Positional binding is therefore an ineffective strategy for solving the visual task.

This creates pressure for the model to discover an alternative: symbolic binding. By learning to match attributes to entities based on semantic identity rather than position, the model can solve the visual task regardless of where objects appear. When the model is subsequently transferred back to text, it retains this symbolic strategy, which proves more robust to distribution shifts than the positional approach it would have learned from text alone.

5.5 The Noise Case: Mixed Mechanisms and Pre-trained LLMs

Let's now consider the case where noise tokens are added. The results are shown in Figure 4. As the figure illustrates, $\mathcal{M}_{\text{noise-text}}$ exhibits a slightly different profile from the pure text model: its binding strategy remains predominantly positional, but with a modest increase in symbolic behavior. Introducing unattendable noise tokens disrupts the clean positional regularities present in the synthetic text data, making strict positional counting less reliable and encouraging the model to rely partially on semantic matching.

This controlled effect mirrors observations in large pre-trained LLMs. Prior work shows that different families of models use a mixture of positional and symbolic mechanisms rather than purely positional strategies Gur-Arieh et al. (2025). Our results suggest a possible explanation: natural language is inherently irregular and less positionally structured than our synthetic task, introducing variability that weakens positional shortcuts and promotes partial symbolic binding. We therefore hypothesize that exposure to unstructured text during pre-training nudges models toward mixed mechanisms.

However, this shift is incomplete. Despite its increased symbolic component, $\mathcal{M}_{\text{noise-text}}$ (57.5% OOD) still substantially underperforms $\mathcal{M}_{\text{image-text}}$ (69.5% OOD), indicating that noise alone does not induce fully robust binding. Visual training appears to exert a stronger and more direct pressure toward symbolic strategies, changing which mechanism is viable rather than merely degrading positional cues.

Consistent with this interpretation, $\mathcal{M}_{\text{noise-image-text}}$ combines both effects: it exhibits symbolic binding similar to $\mathcal{M}_{\text{image-text}}$ yet achieves even higher OOD performance (83.6%). This suggests complementary roles: visual training drives the mechanism shift, and noise exposure further improves generalization, likely through broader positional coverage without altering the dominant binding strategy.

5.6 Validation on Large-Scale Models

To verify that our findings generalize beyond controlled experiments, we performed interchange interventions on the Qwen model family (Qwen 2, 2.5, and 3), employing the same code and task setup as Gur-Arieh et al. (2025). Following their methodology, we identified the layer with the highest intervention effect as the primary binding layer and computed the ratio of symbolic to positional signals.

As shown in Table 1, the VLM variants consistently exhibit a higher symbolic-to-positional ratio than their text-only counterparts. The effect is especially pronounced in Qwen 3, where the VLM attains a symbolic-to-positional ratio of 2.463 compared to 1.819 for the text-only model—a difference of +0.644.

This aligns with the behavioral results in Section 2, where the performance advantage of the VLM on the retrieval tasks was most substantial for Qwen 3. Together, these findings indicate that visual training systematically shifts models toward symbolic binding, and that this shift underlies the improved retrieval performance observed in VLMs. We provide a detailed circuit-level analysis of how these binding mechanisms are implemented in Appendix G.

Our findings suggest that the choice of training modalities and their ordering may fundamentally shape which computational strategies a model discovers. If translation invariance in images drives the shift to symbolic binding, might other modalities with analogous invariances (e.g., pitch invariance in audio, temporal invariance in video) induce similar effects? More speculatively, could synthetic text curricula that artificially introduce translation-like perturbations promote robust binding without requiring visual data at all? The persistence of symbolic binding after returning to text-only training hints at an intriguing asymmetry: some mechanisms, once learned, may be difficult to unlearn. Understanding which training signals reliably induce—and preserve—robust internal strategies could inform the design of more efficient multimodal curricula.

6 Related Work

Multi-modal training effects on language models. Recent work has systematically compared multi-modal training regimes against their language-only backbones to understand how visual grounding reshapes linguistic capabilities. From a theoretical standpoint, multi-modal training has been argued to promote robustness and generalization by discouraging reliance on modality-specific correlations Xue et al. (2024) and by inducing a more faithful and structured latent semantic space Huang et al. (2021). Empirically, several studies show that VLMs can retain or even improve text-only performance, with Dai et al. (2024b) reporting gains in language understanding, mathematics, coding, and reasoning, and Ratzlaff et al. (2025) observing improvements in commonsense reasoning. However, these benefits are not uniform: multi-modal training can also introduce regressions, such as degraded mathematical reasoning in some LLaVA-style models Ratzlaff et al. (2025).

Mechanistic Interpretability. We adopt a mechanistic interpretability perspective to analyze Transformer internals, using interchange interventions Meng et al. (2022); Geiger et al. (2021); Finlayson et al. (2021) to causally identify which hidden activations drive outputs and how binding information is propagated Feng & Steinhardt (2024); Gur-Arieh et al. (2025); Wu et al. (2025).

Binding. Binding—the ability to correctly associate entities with their attributes Treisman (1996); Feng & Steinhardt (2024)—has recently been examined through mechanistic analyses that probe how Transformers implement and represent such associations. Prior work has leveraged interchange interventions Feng & Steinhardt (2024); Saravanan et al. (2025); Gur-Arieh et al. (2025); Prakash et al. (2025); Wu et al. (2025) and analyses of attention head behavior Wu et al. (2025); Urrutia et al. (2025) to characterize how binding information is encoded, propagated, and learned within the network Wu et al. (2025). We build directly on this line of research, grounding our analysis in the taxonomy of binding mechanisms introduced by Gur-Arieh et al. (2025), which distinguishes between positional Dai et al. (2024a); Prakash et al. (2024; 2025), symbolic, and reflexive binding, and use it as a unifying framework to interpret the binding behaviors observed in our models.

7 Conclusion

We showed that visual training improves text-only retrieval by inducing a shift from positional to symbolic binding. This shift, observed in both controlled experiments and pretrained VLMs, accounts for improved OOD generalization. Our findings suggest cross-modal training acts as an inductive bias toward more robust internal computations—even when evaluation is unimodal. This points to an underexplored benefit of multimodal learning: the internal mechanisms shaped by one modality can transfer to improve performance on another.

More broadly, multimodal objectives may offer a principled way to mitigate shortcut learning and strengthen generalization. An intriguing open question is whether other modalities with analogous invariances—such as pitch invariance in audio or temporal invariance in video—might induce similar beneficial shifts. Future work should identify which modality properties most effectively drive these representational changes, and whether such effects can be achieved through synthetic data augmentations alone. For practitioners, our results highlight that the order and composition of training modalities may matter as much as the data itself—a consideration that deserves attention when designing multimodal training pipelines.

REFERENCES

Janice Ahn, Rishu Verma, Renze Lou, Di Liu, Rui Zhang, and Wenpeng Yin. Large language models for mathematical reasoning: Progresses and challenges. In *Proceedings of the 18th Conference of the European Chapter of the Association for Computational Linguistics: Student Research Workshop*, pp. 225–237, 2024.

Guillaume Alain and Yoshua Bengio. Understanding intermediate layers using linear classifier probes, 2017. URL https://openreview.net/forum?id=ryF7rTqgl.

Jean-Baptiste Alayrac, Jeff Donahue, Pauline Luc, Antoine Miech, Iain Barr, Yana Hasson, Karel Lenc, Arthur Mensch, Katherine Millican, Malcolm Reynolds, et al. Flamingo: a visual language model for few-shot learning. *Advances in neural information processing systems*, 35:23716–23736, 2022.

Jinze Bai, Shuai Bai, Shusheng Yang, Shijie Wang, Sinan Tan, Peng Wang, Junyang Lin, Chang Zhou, and Jingren Zhou. Qwen-vl: A versatile vision-language model for understanding, localization, text reading, and beyond, 2023. URL https://arxiv.org/abs/2308.12966.

Joost Bastings, Marco Baroni, Jason Weston, Kyunghyun Cho, and Douwe Kiela. Jump to better conclusions: Scan both left and right. *arXiv preprint arXiv:1809.04640*, 2018.

Yonatan Belinkov. Probing classifiers: Promises, shortcomings, and advances. *Computational Linguistics*, 48(1):207–219, March 2022. doi: 10.1162/coli_a_00422. URL https://aclanthology.org/2022.cl-1.7/.

Tom Brown, Benjamin Mann, Nick Ryder, Melanie Subbiah, Jared D Kaplan, Prafulla Dhariwal, Arvind Neelakantan, Pranav Shyam, Girish Sastry, Amanda Askell, Sandhini Agarwal, Ariel Herbert-Voss, Gretchen Krueger, Tom Henighan, Rewon Child, Aditya Ramesh, Daniel Ziegler, Jeffrey Wu, Clemens Winter, Chris Hesse, Mark Chen, Eric Sigler, Mateusz Litwin, Scott Gray, Benjamin Chess, Jack Clark, Christopher Berner, Sam McCandlish, Alec Radford, Ilya Sutskever, and Dario Amodei. Language models are few-shot learners. In H. Larochelle, M. Ranzato, R. Hadsell, M.F. Balcan, and H. Lin (eds.), *Advances in Neural Information Processing Systems*, volume 33, pp. 1877–1901. Curran Associates, Inc., 2020. URL https://proceedings.neurips.cc/paper_files/paper/2020/file/1457c0d6bfcb4967418bfb8ac142f64a-Paper.pdf.

Avi Cooper, Keizo Kato, Chia-Hsien Shih, Hiroaki Yamane, Kasper Vinken, Kentaro Takemoto, Taro Sunagawa, Hao-Wei Yeh, Jin Yamanaka, Ian Mason, et al. Rethinking vlms and llms for image classification. *Scientific Reports*, 15(1):19692, 2025.

Róbert Csordás, Kazuki Irie, and Juergen Schmidhuber. The devil is in the detail: Simple tricks improve systematic generalization of transformers. In *Proceedings of the 2021 Conference on Empirical Methods in Natural Language Processing*, pp. 619–634, Online and Punta Cana, Dominican Republic, November 2021. Association for Computational Linguistics. doi: 10.18653/v1/2021.emnlp-main.49. URL https://aclanthology.org/2021.emnlp-main.49.

Qin Dai, Benjamin Heinzerling, and Kentaro Inui. Representational analysis of binding in language models. In *2024 Conference on Empirical Methods in Natural Language Processing, EMNLP 2024*, pp. 17468–17493. Association for Computational Linguistics (ACL), 2024a.

Wenliang Dai, Nayeon Lee, Boxin Wang, Zhuoling Yang, Zihan Liu, Jon Barker, Tuomas Rintamaki, Mohammad Shoeybi, Bryan Catanzaro, and Wei Ping. Nvlm: Open frontier-class multimodal llms. *CoRR*, 2024b.

Jacob Devlin, Ming-Wei Chang, Kenton Lee, and Kristina Toutanova. BERT: Pre-training of deep bidirectional transformers for language understanding. In Jill Burstein, Christy Doran, and Thamar Solorio (eds.), *Proceedings of the 2019 Conference of the North American Chapter of the Association for Computational Linguistics: Human Language Technologies, Volume 1 (Long and Short Papers)*, pp. 4171–4186, Minneapolis, Minnesota, June 2019. Association for Computational Linguistics. doi: 10.18653/v1/N19-1423. URL https://aclanthology.org/N19-1423/.

Alexey Dosovitskiy, Lucas Beyer, Alexander Kolesnikov, Dirk Weissenborn, Xiaohua Zhai, Thomas Unterthiner, Mostafa Dehghani, Matthias Minderer, Georg Heigold, Sylvain Gelly, Jakob Uszkoreit, and Neil Houlsby. An image is worth 16x16 words: Transformers for image recognition at scale. In *International Conference on Learning Representations*, 2021. URL https://openreview.net/forum?id=YicbFdNTTy.

Jiahai Feng and Jacob Steinhardt. How do language models bind entities in context? In *The Twelfth International Conference on Learning Representations*, 2024. URL https://openreview.net/forum?id=zb3b6oKO77.

Matthew Finlayson, Aaron Mueller, Sebastian Gehrmann, Stuart M Shieber, Tal Linzen, and Yonatan Belinkov. Causal analysis of syntactic agreement mechanisms in neural language models. In *Proceedings of the 59th Annual Meeting of the Association for Computational Linguistics and the 11th International Joint Conference on Natural Language Processing (Volume 1: Long Papers)*, pp. 1828–1843, 2021.

Atticus Geiger, Kyle Richardson, and Christopher Potts. Neural natural language inference models partially embed theories of lexical entailment and negation. In *Proceedings of the Third BlackboxNLP Workshop on Analyzing and Interpreting Neural Networks for NLP*, pp. 163–173, 2020.

Atticus Geiger, Hanson Lu, Thomas Icard, and Christopher Potts. Causal abstractions of neural networks. *Advances in Neural Information Processing Systems*, 34:9574–9586, 2021.

Robert Geirhos, Jörn-Henrik Jacobsen, Claudio Michaelis, Richard Zemel, Wieland Brendel, Matthias Bethge, and Felix A Wichmann. Shortcut learning in deep neural networks. *Nature Machine Intelligence*, 2(11):665–673, 2020.

Mor Geva, Jasmijn Bastings, Katja Filippova, and Amir Globerson. Dissecting recall of factual associations in auto-regressive language models. In *Proceedings of the 2023 Conference on Empirical Methods in Natural Language Processing*, pp. 12216–12235, 2023.

Yoav Gur-Arieh, Mor Geva, and Atticus Geiger. Mixing mechanisms: How language models retrieve bound entities in-context. *arXiv preprint arXiv:2510.06182*, 2025.

Kaiming He, Xiangyu Zhang, Shaoqing Ren, and Jian Sun. Deep residual learning for image recognition. In *Proceedings of the IEEE conference on computer vision and pattern recognition*, pp. 770–778, 2016.

Yu Huang, Chenzhuang Du, Zihui Xue, Xuanyao Chen, Hang Zhao, and Longbo Huang. What makes multi-modal learning better than single (provably). *Advances in Neural Information Processing Systems*, 34:10944–10956, 2021.

Samy Jelassi, Stéphane d'Ascoli, Carles Domingo-Enrich, Yuhuai Wu, Yuanzhi Li, and François Charton. Length generalization in arithmetic transformers. *arXiv preprint arXiv:2306.15400*, 2023.

Brenden Lake and Marco Baroni. Generalization without systematicity: On the compositional skills of sequence-to-sequence recurrent networks. In *International conference on machine learning*, pp. 2873–2882. PMLR, 2018.

Junnan Li, Dongxu Li, Silvio Savarese, and Steven Hoi. Blip-2: Bootstrapping language-image pre-training with frozen image encoders and large language models. In *International conference on machine learning*, pp. 19730–19742. PMLR, 2023.

Haotian Liu, Chunyuan Li, Qingyang Wu, and Yong Jae Lee. Visual instruction tuning. *Advances in neural information processing systems*, 36:34892–34916, 2023.

Nelson F Liu, Kevin Lin, John Hewitt, Ashwin Paranjape, Michele Bevilacqua, Fabio Petroni, and Percy Liang. Lost in the middle: How language models use long contexts. *Transactions of the association for computational linguistics*, 12:157–173, 2024.

Kevin Meng, David Bau, Alex Andonian, and Yonatan Belinkov. Locating and editing factual associations in gpt. In S. Koyejo, S. Mohamed, A. Agarwal, D. Belgrave, K. Cho, and A. Oh (eds.), *Advances in Neural Information Processing Systems*, volume 35, pp. 17359–17372. Curran Associates, Inc., 2022. URL https://proceedings.neurips.cc/paper_files/paper/2022/file/6f1d43d5a82a37e89b0665b33bf3a182-Paper-Conference.pdf.

Nikhil Prakash, Tamar Rott Shaham, Tal Haklay, Yonatan Belinkov, and David Bau. Fine-tuning enhances existing mechanisms: A case study on entity tracking. In *The Twelfth International Conference on Learning Representations*, 2024. URL https://openreview.net/forum?id=8sKcAWOf2D.

Nikhil Prakash, Natalie Shapira, Arnab Sen Sharma, Christoph Riedl, Yonatan Belinkov, Tamar Rott Shaham, David Bau, and Atticus Geiger. Language models use lookbacks to track beliefs, 2025. URL https://arxiv.org/abs/2505.14685.

Neale Ratzlaff, Man Luo, Xin Su, Vasudev Lal, and Phillip Howard. Training-free mitigation of language reasoning degradation after multimodal instruction tuning. In *Proceedings of the AAAI Symposium Series*, volume 5, pp. 384–388, 2025.

Abhilasha Ravichander, Yonatan Belinkov, and Eduard Hovy. Probing the probing paradigm: Does probing accuracy entail task relevance? In Paola Merlo, Jorg Tiedemann, and Reut Tsarfaty (eds.), *Proceedings of the 16th Conference of the European Chapter of the Association for Computational Linguistics: Main Volume*, pp. 3363–3377, Online, April 2021. Association for Computational Linguistics. doi: 10.18653/v1/2021.eacl-main.295. URL https://aclanthology.org/2021.eacl-main.295/.

Laura Ruis, Jacob Andreas, Marco Baroni, Diane Bouchacourt, and Brenden M Lake. A benchmark for systematic generalization in grounded language understanding. *Advances in Neural Information Processing Systems*, 33, 2020.

Abulhair Saparov, Richard Yuanzhe Pang, Vishakh Padmakumar, Nitish Joshi, Mehran Kazemi, Najoung Kim, and He He. Testing the general deductive reasoning capacity of large language models using ood examples. *Advances in Neural Information Processing Systems*, 36:3083–3105, 2023.

Darshana Saravanan, Makarand Tapaswi, and Vineet Gandhi. Investigating mechanisms for in-context vision language binding. In *Proceedings of the IEEE/CVF Conference on Computer Vision and Pattern Recognition (CVPR) Workshops*, pp. 4891–4895, June 2025.

Ruoqi Shen, Sébastien Bubeck, Ronen Eldan, Yin Tat Lee, Yuanzhi Li, and Yi Zhang. Positional description matters for transformers arithmetic. *arXiv preprint arXiv:2311.14737*, 2023.

Oriane Siméoni, Huy V. Vo, Maximilian Seitzer, Federico Baldassarre, Maxime Oquab, Cijo Jose, Vasil Khalidov, Marc Szafraniec, Seungeun Yi, Michaël Ramamonjisoa, Francisco Massa, Daniel Haziza, Luca Wehrstedt, Jianyuan Wang, Timothée Darcet, Théo Moutakanni, Leonel Sentana, Claire Roberts, Andrea Vedaldi, Jamie Tolan, John Brandt, Camille Couprie, Julien Mairal, Hervé Jégou, Patrick Labatut, and Piotr Bojanowski. Dinov3, 2025. URL https://arxiv.org/abs/2508.10104.

Jianlin Su, Murtadha Ahmed, Yu Lu, Shengfeng Pan, Wen Bo, and Yunfeng Liu. Roformer: Enhanced transformer with rotary position embedding. *Neurocomputing*, 568:127063, 2024.

A. Treisman. The binding problem. 6(2):171–178, 1996. ISSN 0959-4388. doi: 10.1016/s0959-4388(96)80070-5.

Felipe Urrutia, Jorge Salas, Alexander Kozachinskiy, Cristian Buc Calderon, Hector Pasten, and Cristobal Rojas. Decoupling positional and symbolic attention behavior in transformers. *arXiv preprint arXiv:2511.11579*, 2025.

Jesse Vig, Sebastian Gehrmann, Yonatan Belinkov, Sharon Qian, Daniel Nevo, Yaron Singer, and Stuart Shieber. Investigating gender bias in language models using causal mediation analysis. *Advances in neural information processing systems*, 33:12388–12401, 2020.

Jason Wei, Xuezhi Wang, Dale Schuurmans, Maarten Bosma, Fei Xia, Ed Chi, Quoc V Le, Denny Zhou, et al. Chain-of-thought prompting elicits reasoning in large language models. *Advances in neural information processing systems*, 35:24824–24837, 2022.

Bichen Wu, Chenfeng Xu, Xiaoliang Dai, Alvin Wan, Peizhao Zhang, Zhicheng Yan, Masayoshi Tomizuka, Joseph Gonzalez, Kurt Keutzer, and Peter Vajda. Visual transformers: Token-based image representation and processing for computer vision. *arXiv preprint arXiv:2006.03677*, 2020.

Yiwei Wu, Atticus Geiger, and Raphaël Millière. How do transformers learn variable binding in symbolic programs? In *Forty-second International Conference on Machine Learning*, 2025. URL https://openreview.net/forum?id=kVtyv7bpnw.

Yihao Xue, Siddharth Joshi, Dang Nguyen, and Baharan Mirzasoleiman. Understanding the robustness of multi-modal contrastive learning to distribution shift. In *The Twelfth International Conference on Learning Representations*, 2024. URL https://openreview.net/forum?id=rtl4XnJYBh.

An Yang, Baosong Yang, Binyuan Hui, Bo Zheng, Bowen Yu, Chang Zhou, Chengpeng Li, Chengyuan Li, Dayiheng Liu, Fei Huang, Guanting Dong, Haoran Wei, Huan Lin, Jialong Tang, Jialin Wang, Jian Yang, Jianhong Tu, Jianwei Zhang, Jianxin Ma, Jin Xu, Jingren Zhou, Jinze Bai, Jinzheng He, Junyang Lin, Kai Dang, Keming Lu, Keqin Chen, Kexin Yang, Mei Li, Mingfeng Xue, Na Ni, Pei Zhang, Peng Wang, Ru Peng, Rui Men, Ruize Gao, Runji Lin, Shijie Wang, Shuai Bai, Sinan Tan, Tianhang Zhu, Tianhao Li, Tianyu Liu, Wenbin Ge, Xiaodong Deng, Xiaohuan Zhou, Xingzhang Ren, Xinyu Zhang, Xipin Wei, Xuancheng Ren, Yang Fan, Yang Yao, Yichang Zhang, Yu Wan, Yunfei Chu, Yuqiong Liu, Zeyu Cui, Zhenru Zhang, and Zhihao Fan. Qwen2 technical report. *arXiv preprint arXiv:2407.10671*, 2024.

An Yang, Anfeng Li, Baosong Yang, Beichen Zhang, Binyuan Hui, Bo Zheng, Bowen Yu, Chang Gao, Chengen Huang, Chenxu Lv, Chujie Zheng, Dayiheng Liu, Fan Zhou, Fei Huang, Feng Hu, Hao Ge, Haoran Wei, Huan Lin, Jialong Tang, Jian Yang, Jianhong Tu, Jianwei Zhang, Jianxin Yang, Jiaxi Yang, Jing Zhou, Jingren Zhou, Junyang Lin, Kai Dang, Keqin Bao, Kexin Yang, Le Yu, Lianghao Deng, Mei Li, Mingfeng Xue, Mingze Li, Pei Zhang, Peng Wang, Qin Zhu, Rui Men, Ruize Gao, Shixuan Liu, Shuang Luo, Tianhao Li, Tianyi Tang, Wenbiao Yin, Xingzhang Ren, Xinyu Wang, Xinyu Zhang, Xuancheng Ren, Yang Fan, Yang Su, Yichang Zhang, Yinger Zhang, Yu Wan, Yuqiong Liu, Zekun Wang, Zeyu Cui, Zhenru Zhang, Zhipeng Zhou, and Zihan Qiu. Qwen3 technical report, 2025a. URL https://arxiv.org/abs/2505.09388.

An Yang, Baosong Yang, Beichen Zhang, Binyuan Hui, Bo Zheng, Bowen Yu, Chengyuan Li, Dayiheng Liu, Fei Huang, Haoran Wei, Huan Lin, Jian Yang, Jianhong Tu, Jianwei Zhang, Jianxin Yang, Jiaxi Yang, Jingren Zhou, Junyang Lin, Kai Dang, Keming Lu, Keqin Bao, Kexin Yang, Le Yu, Mei Li, Mingfeng Xue, Pei Zhang, Qin Zhu, Rui Men, Runji Lin, Tianhao Li, Tianyi Tang, Tingyu Xia, Xingzhang Ren, Xuancheng Ren, Yang Fan, Yang Su, Yichang Zhang, Yu Wan, Yuqiong Liu, Zeyu Cui, Zhenru Zhang, and Zihan Qiu. Qwen2.5 technical report, 2025b. URL https://arxiv.org/abs/2412.15115.

Jingyi Zhang, Jiaxing Huang, Sheng Jin, and Shijian Lu. Vision-language models for vision tasks: A survey. *IEEE transactions on pattern analysis and machine intelligence*, 46(8):5625–5644, 2024a.

Tianyi Zhang, Faisal Ladhak, Esin Durmus, Percy Liang, Kathleen McKeown, and Tatsunori B Hashimoto. Benchmarking large language models for news summarization. *Transactions of the Association for Computational Linguistics*, 12:39–57, 2024b.

Yi Zhang, Arturs Backurs, Sébastien Bubeck, Ronen Eldan, Suriya Gunasekar, and Tal Wagner. Unveiling transformers with lego: a synthetic reasoning task. *arXiv preprint arXiv:2206.04301*, 2022.

Hattie Zhou, Arwen Bradley, Etai Littwin, Noam Razin, Omid Saremi, Joshua M. Susskind, Samy Bengio, and Preetum Nakkiran. What algorithms can transformers learn? a study in length generalization. In *The Twelfth International Conference on Learning Representations*, 2024a. URL https://openreview.net/forum?id=AssIuHnmHX.

Yongchao Zhou, Uri Alon, Xinyun Chen, Xuezhi Wang, Rishabh Agarwal, and Denny Zhou. Transformers can achieve length generalization but not robustly. In *ICLR 2024 Workshop on Mathematical and Empirical Understanding of Foundation Models*, 2024b. URL https://openreview.net/forum?id=DWkWIh3vFJ.

A DETAILED QWEN PERFORMANCE BREAKDOWN

Figure 5 presents the full performance breakdown for all Qwen model generations. The top row shows Direct Retrieval performance, while the bottom row shows Indirect Retrieval performance. Across all generations, the VLM variants maintain higher accuracy at longer context lengths compared to their text-only counterparts.

B DETAILED PRE-TRAINED MODELS RESULTS

This appendix provides details on the evaluation setup for the pre-trained model experiments presented in Section 2.

Models. We evaluated three generations of Qwen models, comparing their text-only (Instruct) and vision-language (VL-Instruct) variants:

- **Qwen 2**: `Qwen2-7B-Instruct` and `Qwen2-VL-7B-Instruct`
- **Qwen 2.5**: `Qwen2.5-7B-Instruct` and `Qwen2.5-VL-7B-Instruct`
- **Qwen 3**: `Qwen3-8B` and `Qwen3-VL-8B-Instruct`

Inference Setup. All models were loaded using the HuggingFace Transformers library at full precision on a single NVIDIA RTX 3090 GPU. We used each model's default inference settings without modifying temperature or sampling parameters. Prompts were formatted using the model's chat template with the default system prompt ("You are a helpful assistant.").

Evaluation Protocol. For each query, we checked whether the model's generated output contained the correct city name. We report mean accuracy and standard error across all query positions for each context length.

C TASK DETAILS

This appendix provides implementation details for the Indirect Retrieval task introduced in Section 3.

Vocabulary. We define three disjoint vocabularies for the task:

- **Colors:** The full vocabulary consists of 216 colors from the web-safe color palette, formed by a $6 \times 6 \times 6$ RGB grid using hexadecimal values `00`, `33`, `66`, `99`, `cc`, and `ff` for each channel. During image-modality training, we restrict to the first 8 colors. In the text modality, colors are represented as tokens `color0001` through `color0216`.
- **Shapes:** We use 13 distinct shapes: rectangle, circle, hexagon, triangle, pentagon, rhombus, octagon, star, heart, semicircle, cross, arrow, and annulus. In the text modality, shapes are represented as tokens `shape0001` through `shape0013`.
- **Items:** Target labels are represented as tokens `item0001`, `item0002`, etc. Training uses up to 32 distinct items.

Prompt Structure. Both modalities share a common prompt structure with the following special tokens:

- `[CONTEXTEND]` separates the context (attribute-entity pairs) from the association list.
- `[SEP]` separates individual entity-item associations.
- `[QUESTION]` marks the beginning of the query.
- `[ANSWER]` precedes the target output position.

An example text-modality prompt with 3 objects is:

```
color0113 shape0055 color0119 shape0041 color0153 shape0091
[CONTEXTEND] shape0041 item0029 [SEP] shape0055 item0025
[SEP] shape0091 item0020 [QUESTION] color0119 [ANSWER]
```

Here, the query asks for the item associated with `color0119`. Since `color0119` is paired with `shape0041` in the context, and `shape0041` maps to `item0029`, the correct answer is `item0029`.

In the image modality, the context is replaced by a sequence of image tokens extracted from a frozen encoder (e.g., 196 tokens per image for ViT-based encoders), while the associations and query remain in text.

Image Rendering. For the image modality, each colored shape is rendered as a 224×224 pixel image. Shapes are drawn as filled SVG graphics on a white background. Figure 6 shows example renderings of colored shapes used as visual context.

Feature Grounding Task. In addition to the main Indirect Retrieval task, we use an auxiliary *Feature Grounding* task to stabilize training and disentangle reasoning failures from perceptual failures. This simpler task requires the model to directly map an attribute to its corresponding entity without the intermediate item-retrieval step. Given a context of attribute-entity pairs and a query attribute, the model must output the associated entity.

An example text-modality prompt is:

```
color0022 shape0192 color0054 shape0209 [CONTEXTEND]
[QUESTION] color0022 [ANSWER]
```

The correct answer is `shape0192`. In the image modality, the context is similarly replaced by image tokens while the query remains in text.

Symmetric Variations. We consider symmetric variations of both tasks where the roles of entity and attribute are interchangeable. Specifically, we include both configurations: querying by color to retrieve a shape, and querying by shape to retrieve a color. For the Indirect Retrieval task, this extends to assigning items to shapes (retrieved via color) versus assigning items to colors (retrieved via shape). This symmetric formulation is used during training to increase data diversity. All evaluation results reported in the main text use the color-to-shape query direction.

D Detailed Train Procedure

In the previous section, we demonstrated that Vision-Language Models consistently outperform their text-only counterparts on retrieval tasks, particularly as context length increases. To understand the underlying mechanisms driving this phenomenon, we now replicate these findings in a controlled experimental setting. By training small transformers from scratch on our synthetic indirect retrieval task, we gain the ability to apply mechanistic interpretability tools and isolate the factors responsible for improved generalization.

D.1 Model Architecture

We use a 12-layer decoder-only Transformer with the architecture detailed in Table 2. The model employs Rotary Positional Embeddings (RoPE) Su et al. (2024) applied to the query and key projections, using a fixed base frequency of $\theta = 10000$ with interleaved rotation on even and odd dimension pairs. The vocabulary consists of approximately 1000 tokens, covering all color and shape combinations used in our experiments.

D.2 Training Configuration

All models are trained using the AdamW optimizer with a learning rate of 1×10^{-4}, no weight decay, and gradient clipping with a maximum norm of 1.0. We use a batch size of 32 and train with bf16 mixed precision. The learning rate schedule consists of a 2000-step linear warmup followed

Table 2: Model architecture hyperparameters.

Hyperparameter	**Value**
Number of layers	12
Hidden dimension (d_{model})	128
FFN dimension (d_{ff})	512
Attention heads	4
Positional encoding	RoPE ($\theta = 10000$)
Dropout	0
Vocabulary size	$\sim$1000

by a constant learning rate. Training continues until validation performance plateaus, using early stopping with a patience of 10 on the validation set. Experiments were conducted on NVIDIA A6000 and A40 GPUs.

D.3 Text-Only Baseline

We begin by establishing a baseline model trained on the 1-hop indirect retrieval task defined in Section 3. We train exclusively on the text modality, where the context $\mathbf{X}_{\text{context}}^{\text{text}}$ consists of sequential token pairs representing attribute-entity associations (e.g., "red triangle", "blue circle").

Training a Transformer to solve this task from scratch is highly unstable due to the sparsity of the supervision signal. Since the intermediate tokens in the prompt are randomized or independent of the context, the model can only be trained to predict the final answer token. This means there is no direct reward for uncovering the intermediate logical steps (grounding and retrieval), requiring the model to discover the entire reasoning chain at once without partial credit for partial logic. To address this, we employ a five-stage curriculum to incrementally increase task complexity:

1. **Fixed Layout:** Two object pairs, restricted vocabulary (8 colors, 8 shapes), and fixed prompt order (Context $\rightarrow$ Bindings).
2. **Vocabulary Expansion:** Vocabulary increases to 216 colors and 216 shapes, while structure remains fixed.
3. **Variable Length:** Random sampling of 2 to 8 object pairs per prompt.
4. **Randomized Order:** Shuffling of pairs within the context and binding sections to prevent positional memorization.
5. **Scale:** Context capacity increased to support up to 32 items.

We denote the resulting model as $\mathcal{M}_{\text{text-only}}$. To ensure reliability, we repeated this full training curriculum using 4 distinct random seeds. For the experiments, we report the average performance across 4 seeds and the standard error (SE).

As shown in Figure 3, $\mathcal{M}_{\text{text-only}}$ (blue curve) generalizes poorly to OOD sequence lengths. Accuracy drops sharply beyond the training maximum of 8 items, resulting in an average OOD accuracy of 37.2% (SE: 4.0%).

D.4 Noise Training

After completing the text curriculum, we continue training $\mathcal{M}_{\text{text-only}}$ with noise augmentation to extend its positional range. We insert 100 unattendable noise tokens between each context pair, exposing the model to longer positional indices without adding semantic information. The augmented context is formulated as:

$$\mathbf{X}_{\text{context}}^{\text{noise}} = [a_1, e_1, \underbrace{[\text{noise}], \ldots, [\text{noise}]}_{100}, a_2, e_2, \ldots, a_N, e_N]$$

This produces $\mathcal{M}_{\text{noise-text}}$. As shown in Figure 3 (orange curve), noise augmentation substantially improves OOD generalization, increasing average accuracy from 37.2% to 57.5% (SE: 6.8%).

Critically, noise training serves as a prerequisite for the image training pipeline described below. By extending the model's positional range, noise training enables the model to skip the curriculum stages when training on images, where patch tokens naturally produce longer sequences.

D.5 Feature Grounding Pre-training

Before proceeding to image training, we train $\mathcal{M}_{\text{noise-text}}$ on the Feature Grounding auxiliary task in text mode. This task trains the model to predict associations in both directions: given an attribute, predict its associated entity (e.g., given "red", predict "triangle"), and vice versa. This establishes the structural requirements needed for the indirect retrieval task before introducing visual inputs.

D.6 Image Training

Following the Feature Grounding pre-training, we train on the indirect retrieval task in the vision modality. Images are rendered at 224×224 resolution using SVG-based rendering, where each entity is depicted with its corresponding attribute (e.g., colored shapes on a canvas).

Image Encoders. We experiment with three frozen pre-trained image encoders:

- **ResNet-152** He et al. (2016): A supervised CNN producing 2048-dimensional spatial feature maps from the final convolutional stage. We discard global average pooling and fully connected layers, flattening the feature maps to produce pseudo-patch embeddings.
- **ViT-B/16** Wu et al. (2020): A supervised Transformer producing 768-dimensional patch embeddings. We use features from the final layer, discarding the [CLS] token.
- **DINOv3** Siméoni et al. (2025): A self-supervised Transformer producing 768-dimensional patch embeddings. We discard both [CLS] and register tokens to preserve spatial correspondence.

Visual Projector. To map visual representations into the language model's embedding space, we employ a 3-layer MLP projector with a hidden dimension multiplier of $4\times$ (i.e., if the encoder outputs d_{enc}-dimensional features, the hidden layer has dimension $4 \cdot d_{\text{enc}}$). We maintain a strict one-to-one mapping where each visual patch is projected to a single token, without pooling. The resulting features are normalized via LayerNorm both before and after projection, and scaled by $1/\sqrt{d_{\text{model}}}$ before concatenation into the input sequence.

Training. We train on image prompts, jointly optimizing for both 1-hop retrieval and Feature Grounding. For training stability, this stage uses a restricted distribution (8 colors, 13 shapes, up to 8 items), yielding $\mathcal{M}_{\text{image}}$.

D.7 Text Transfer and Vocabulary Expansion

After image training, we transfer the model back to the text domain in two stages:

Mixed Modality Training. We train on a 20/80 split of image and text tasks, maintaining the restricted vocabulary (8 colors, 13 shapes). This produces $\mathcal{M}_{\text{image-text-limited}}$.

Vocabulary Expansion. Since the image training uses only 13 shapes (limited by what can be rendered distinguishably), we cannot directly evaluate OOD generalization to 32 items. To enable OOD evaluation, we continue training $\mathcal{M}_{\text{image-text-limited}}$ on text-only data, expanding the distribution to match the full complexity of the baseline (216 colors, 216 shapes, up to 32 items). This produces our final model $\mathcal{M}_{\text{image-text}}$.

Noise Augmentation (Optional). To further improve generalization, we can apply noise training to $\mathcal{M}_{\text{image-text}}$, producing $\mathcal{M}_{\text{noise-image-text}}$.

D.8 EXPERIMENTAL SETUP

We conducted experiments using 4 random seeds. For each seed, we trained separate versions of $\mathcal{M}_{\text{image}}$ using each of the three image encoders (ResNet-152, DINOv3, ViT), resulting in a total of 12 experimental runs (4 seeds $\times$ 3 encoders). We report aggregated performance across these runs, excluding a single divergent run (Seed 2 with ViT encoder).

As shown in Figure 3, $\mathcal{M}_{\text{image-text}}$ (green curve) exhibits significantly improved performance over the text-only baseline, achieving an average accuracy of 69.5% (SE: 3.3%). This substantial improvement demonstrates that visual training enhances text-based generalization, replicating the phenomenon observed in large-scale VLMs.

D.9 ANALYSIS: CONTEXT LENGTH VS. VISUAL TRAINING

The superior performance of $\mathcal{M}_{\text{image-text}}$ raises a natural question: *Why does visual training improve text-based generalization?* One hypothesis is that the improvement stems from exposure to longer sequences during visual training. Since image encoders produce sequences of patch tokens (e.g., 196 tokens for a 14×14 patch grid), the model encounters a broader range of positional indices compared to text-only training.

To test whether context length exposure alone explains the performance gap, we compare models with and without noise augmentation (described in Section D.4). The noise-augmented text model $\mathcal{M}_{\text{noise-text}}$ achieves 57.5% average OOD accuracy, while the image-text model $\mathcal{M}_{\text{image-text}}$ achieves 69.5%. Applying noise augmentation to the image-text model yields $\mathcal{M}_{\text{noise-image-text}}$ at 83.6%.

Critically, even with noise augmentation, $\mathcal{M}_{\text{noise-text}}$ (57.5%) remains substantially worse than $\mathcal{M}_{\text{image-text}}$ without noise (69.5%). This demonstrates that while exposure to longer positional ranges helps, it is insufficient to fully explain the generalization advantages conferred by visual training. The visual modality must provide qualitatively different inductive biases beyond simple context length expansion.

D.10 KEY FINDINGS

The controlled experiments presented in this section reveal several critical insights:

- Text-only models trained on short contexts exhibit poor OOD generalization (37.2% average accuracy on longer sequences).
- Visual training substantially improves generalization (69.5%), replicating the VLM advantage observed in large-scale models.
- Noise augmentation, which exposes models to longer positional ranges, provides substantial improvement to text-only models (57.5%), but remains insufficient to match multimodal performance.
- Even after noise augmentation, the vision-trained model maintains superior performance, suggesting that visual training induces qualitatively different computational mechanisms beyond positional range expansion.
- Combining visual training with noise augmentation yields the strongest performance (83.6%), suggesting complementary regularization effects.

These findings demonstrate that the benefits of multimodal training extend beyond simple exposure to longer sequences. The critical question remains: *What underlying computational mechanism does visual training induce that enables superior generalization?* In the following section, we employ mechanistic interpretability techniques to reveal that the answer lies in a fundamental shift in how models bind and retrieve information—transitioning from brittle positional strategies to robust identity-based binding mechanisms.

E Detailed Accuracy Sweeps (Scratch Models)

Figure 7 shows individual generalization curves for each scratch model variant. Models trained with meaningful visual input ($\mathcal{M}_{\text{image-text}}$) generalize beyond the training distribution, while text-only and noise-augmented variants show sharp accuracy drops at longer sequence lengths.

F Detailed Interchange Results

We performed interchange interventions across 4 random seeds for the Text-Only model and 11 runs (across 3 encoders) for the Image-Text model. Figure 8 illustrates the consistency of the mechanism type despite variations in circuit depth.

It is important to note that the model can be marked as "Reflexive" if the answer is already stored in its activations from a previous step. In this context, the Reflexive signal represents a readout of stored information rather than the retrieval process. Therefore, the critical indicator of the binding mechanism is the *first* spike in causal effect.

G Detailed Circuit Analysis

This section provides detailed analysis of how each binding mechanism operates at the circuit level. We use attention knockouts to identify critical token-to-token connections and linear probes to trace information flow through the network. Together, these reveal the computational structure underlying each mechanism. Figure 9 illustrates the information flow in each circuit type.

The Positional Circuit. The circuit operates in two independent streams: (1) the color query token identifies the position of its matching attribute in the context, and (2) the association shape token independently finds its matching shape and stores that context position. These streams never exchange attribute information—the "binding" is implicit, relying solely on shared position indices. The answer token retrieves the correct item by matching position indices.

Symbolic Circuit A (Color-Key). This variant uses color as the retrieval key. The circuit actively moves content: context color is first copied into the context shape token, creating an explicit attribute-entity bundle. Then, the association shape retrieves this stored color from the context. Finally, both the association item and answer token converge on this color information to produce the correct output.

Symbolic Circuit B (Shape-Key). Similar to Circuit A, the context color is initially copied into the context shape. However, the query color looks back at the context to find the shape token marked with its color, copying the shape context into its activations. The answer token uses this shape information for retrieval.

Despite their different intermediate keys, both symbolic variants share the fundamental property of transferring semantic identity rather than positional indices. This explains the robustness to sequence length observed in our results.

G.1 Methodology

Attention Knockouts. For each source-target token pair, we mask all attention from the source to the target and measure the resulting accuracy drop. High knockout effect indicates that the information flow between those tokens is essential for the task.

Linear Probes. We train lightweight classifiers on residual stream activations to decode position indices, color identity, shape identity, and item identity at each layer and token position. By tracking when and where each type of information becomes decodable, we trace semantic content through the network.

G.2 The Positional Circuit

The text-only model implements binding through position indices rather than semantic content. The knockout and probe results reveal how this works in detail (Figures 10a and 11a).

Step-by-Step Information Flow. The circuit operates through two independent streams that converge at the answer:

1. **Query Stream:** The question token (the color in the query) attends to the matching color in the context section. It copies the *position index* of that context color into its own activations. The `[ANSWER]` token then copies this position from the question token next to it.
2. **Association Stream:** Independently, the shape token in the association section attends to the matching shape in the context section and copies its position index. The item token in the association section then copies this position from the shape token next to it.
3. **Retrieval:** The `[ANSWER]` token looks for the item in the association section that holds the same position index it is holding. When the positions match, retrieval succeeds.

Evidence from Knockouts. The knockout matrix confirms these critical pathways: Question → Context Color (position lookup), Answer → Question (position copy), Association Shape → Context Shape (position lookup), and Association Item → Association Shape (position copy). Notably, there is no critical attention between color and shape tokens—the circuit never routes semantic content between positions.

Evidence from Probes. The probes show position information accumulating at each step: first at the question and association shape tokens (after the lookup), then at the answer and association item tokens (after the copy). Critically, attribute identity (color, shape) remains *undecodable* at entity positions throughout—the model never represents "red circle" as a bound unit. Only position indices are transferred.

This explains why the positional mechanism fails on longer sequences: it relies on position counting, and unfamiliar position indices break the heuristics.

G.3 Symbolic Circuit A (Color-Key)

Image-trained models using the Color-Key variant implement explicit attribute binding (Figures 10b and 11b). Unlike the positional circuit, semantic content—not just position indices—is transferred between tokens.

Step-by-Step Information Flow. The circuit operates through two streams that converge at the answer:

1. **Binding in Context:** The context shape token accumulates the *color identity* from the adjacent context color token. This creates an explicit attribute-entity bundle: the shape now "knows" its color.
2. **Association Stream:** The shape in the association section looks back at the matching shape in the context section and copies the color into its activations. The item in the association section then copies the color from the adjacent shape.
3. **Query Stream:** Independently, the `[ANSWER]` token copies color from the adjacent query (color token).
4. **Retrieval:** The `[ANSWER]` token looks for the item in the association section that has the same color in its activations. When the colors match, retrieval succeeds.

Evidence from Knockouts. The knockout matrix confirms these attribute-routing pathways: Context Shape → Context Color (binding), Association Shape → Context Shape (color retrieval), Association Item → Association Shape (color propagation), and Answer → Query (color copy). These pathways are absent in the positional circuit.

Evidence from Probes. The probes reveal the **binding signature**: color identity first becomes decodable at the context shape token (binding), then at the association shape and item tokens (retrieval and propagation). This confirms that semantic content is being actively moved between tokens.

G.4 Symbolic Circuit B (Shape-Key)

The Shape-Key variant uses a different intermediate representation but achieves the same explicit binding (Figures 10c and 11c).

Step-by-Step Information Flow. The circuit again operates through two streams:

1. **Binding in Context:** As in Circuit A, the context shape token accumulates color identity from the adjacent context color.
2. **Association Stream:** The item in the association section copies the adjacent *shape identity* into its activations.
3. **Query Stream:** Independently, the query (color token) looks back at the context and finds the shape marked with the same color. It copies the *shape identity* into its activations. The `[ANSWER]` token then copies this shape from the adjacent query.
4. **Retrieval:** The `[ANSWER]` token looks for the item in the association section that has the same shape in its activations. When the shapes match, retrieval succeeds.

Evidence from Knockouts. The critical pathways differ from Circuit A: Query → Context Shape is now critical (the query retrieves shape identity), and Association Item → Association Shape (shape propagation).

Evidence from Probes. The binding signature appears with shape identity rather than color. Shape information becomes decodable at the query token after attending to the context shape, then at the `[ANSWER]` token. Despite the different intermediate key, the fundamental property is preserved: semantic content transfers between tokens, enabling length-agnostic retrieval.

G.5 Consistency Across Seeds and Encoders

The patterns are consistent across experimental runs (Figures 12 and 13). All text models exhibit the positional pattern; all image-text models exhibit the symbolic pattern. The specific variant (A vs. B) varies by seed and encoder, but explicit attribute transfer is universal across image-trained runs. This confirms that symbolic binding is a robust emergent property of vision-language training.

G.6 Extension to Large-Scale Models

We extended our analysis to the Qwen model family (Qwen 2, 2.5, and 3). Full circuit analysis via attention knockouts is computationally prohibitive at this scale, so we use linear probes as a proxy: if a model implements symbolic binding, attribute information should become decodable at entity positions.

The VLM variants exhibit the binding signature. Color decodability at entity tokens is consistently higher in VLMs than in their text-only counterparts across the layer ranges where binding occurs. Moreover, the *ordering* of when probes rise coincides with the proposed order of Symbolic Circuit A: color information first becomes decodable at the context shape token, then at the association shape token, reflecting binding in context before propagation through associations. Text-only baselines show low attribute decodability at these positions throughout.

See Appendix H for detailed results. The consistency across model scales suggests symbolic binding is a general property of vision-language training.

H Qwen Probe Results

We present detailed linear probe results for the Qwen model family. Figure 14 shows color decodability at the context shape token, where binding first occurs. Figure 15 shows color decodability at the association shape token, reflecting propagation of bound attributes. Across all three model generations, VLMs consistently show higher color decodability at entity positions than their text-only counterparts.

I Related Work (Extended Version)

Multi-modal training effects on language models. Multi-modal training has been studied by comparing multi-modal models against their original unimodal backbone language models in order

to assess how augmenting them with visual modalities alters their behavior and performance. Several works provide theoretical grounding suggesting that multi-modal training promote robustness and generalization beyond the training distribution, arguing that it discourages reliance on spurious, modality-specific correlations that are over-represented in unimodal training data Xue et al. (2024) and instead promote more faithful estimation of the underlying latent semantic space Huang et al. (2021). Empirically, vision–language models (VLMs) have been shown to retain, and in some cases even improve, strong performance on purely textual tasks. For instance, Dai et al. (2024b) demonstrate that, under appropriate training regimes, a VLM can preserve or enhance the text-only capabilities of its language backbone across benchmarks in language understanding, mathematics, coding, and reasoning, while Ratzlaff et al. (2025) reporting similar findings on commonsense reasoning. However, these effects are highly model- and backbone-dependent: Ratzlaff et al. (2025) show that for LLaVA-style models, multi-modal training can either improve or degrade textual performance depending on the underlying LLM and, in some cases, introduce degradation in mathematical reasoning. Complementarily, studies have also examined the impact in the opposite direction, from language to vision. Cooper et al. (2025) find that while pure VLMs outperform hybrid VLM–LLM systems on perceptual tasks such as object and scene recognition, the inclusion of an LLM yields gains on tasks requiring higher-level reasoning or external knowledge.

Mechanistic interpretability Mechanistic interpretability provides a principled framework for analyzing how neural networks implement computations internally, enabling causal rather than purely correlational explanations of model behavior. In this work, we adopt a suite of complementary interpretability tools to characterize and compare the mechanisms underlying the models we study, before and after image training. First, we employ interchange interventions Meng et al. (2022); Geiger et al. (2021); Finlayson et al. (2021); Vig et al. (2020); Geiger et al. (2020), which causally intervene on hidden states by swapping representations between paired examples, allowing us to identify which internal activations are responsible for specific outputs. This approach is closely related to recent studies on binding and compositional representations in Transformers Feng & Steinhardt (2024); Saravanan et al. (2025); Gur-Arieh et al. (2025); Wu et al. (2025), and enables fine-grained analysis of how information is localized and propagated through the network. Second, we use attention knockout techniques Geva et al. (2023); Gur-Arieh et al. (2025), which selectively zero out attention connections between targeted token pairs, to evaluate how disrupting specific information pathways affects task performance. Finally, we rely on linear probing methods Alain & Bengio (2017); Ravichander et al. (2021); Belinkov (2022), training lightweight classifiers on hidden representations to assess whether particular concepts or variables are linearly decodable, thereby providing insight into what information is encoded at different layers of the model. Together, these tools allow us to causally and representationally dissect the internal computations of Transformers and to connect observed generalization behavior with concrete underlying mechanisms.

Binding Binding refers to a model's ability to correctly associate entities with their corresponding attributes Treisman (1996); Feng & Steinhardt (2024). Recent work has investigated the internal mechanisms by which Transformers implement binding, typically through controlled retrieval tasks that require recovering an attribute given an entity in the query Feng & Steinhardt (2024); Saravanan et al. (2025); Wu et al. (2025); Gur-Arieh et al. (2025); Prakash et al. (2025). These studies intervene on model activations to characterize the information used to form bindings and how these mechanisms evolve during learning, discovering different behaviors that this mechanism shows through training Wu et al. (2025). Using the taxonomy introduced by Gur-Arieh et al. (2025), prior work, distinct binding strategies in language models have been identified, including positional mechanisms that rely on token order or relative position Dai et al. (2024a); Prakash et al. (2024; 2025), symbolic (termed lexical in the original work) mechanisms that exploit content-based cues, and reflexive mechanisms that use a self-referential association between tokens Gur-Arieh et al. (2025). Complementary analyses based on attention patterns further support this view, with Urrutia et al. (2025) providing evidence for both positional and symbolic binding heads in language models trained on retrieval tasks similar to ours. Moreover, detailed studies of attention head behavior reveal the emergence of specialized heads that systematically route information across token positions to facilitate binding operations Wu et al. (2025).

Length generalization A substantial body of work has demonstrated that neural networks often struggle with length generalization, i.e., extrapolating to input lengths longer than those observed

during training, and has introduced benchmarks to systematically evaluate this capability Lake & Baroni (2018); Bastings et al. (2018); Ruis et al. (2020); Zhang et al. (2022); Saparov et al. (2023); Zhou et al. (2024a). In the context of Transformers, these limitations have been observed across a variety of settings, including arithmetic tasks such as summing longer numbers Zhou et al. (2024b), varying the length of chains of reasoning Zhang et al. (2022), deductive reasoning Saparov et al. (2023), and general algorithmic problems Zhou et al. (2024a). Nevertheless, several studies indicate that Transformers can exhibit weak but non-negligible extrapolation under specific conditions. For instance, pre-training has been shown to improve robustness to length extrapolation Zhang et al. (2022), while architectural choices such as relative positional encodings Csordás et al. (2021), NoPE Shen et al. (2023), and the integration of FIRE and randomized positional encodings Zhou et al. (2024b) can mitigate positional overfitting. Complementarily, carefully designed input representations that better align with the underlying task structure have been shown to facilitate length generalization Shen et al. (2023); Zhou et al. (2024b). Finally, even minimal exposure to longer sequences during training, through the inclusion of a small number of long examples, can substantially improve extrapolation performance Jelassi et al. (2023).

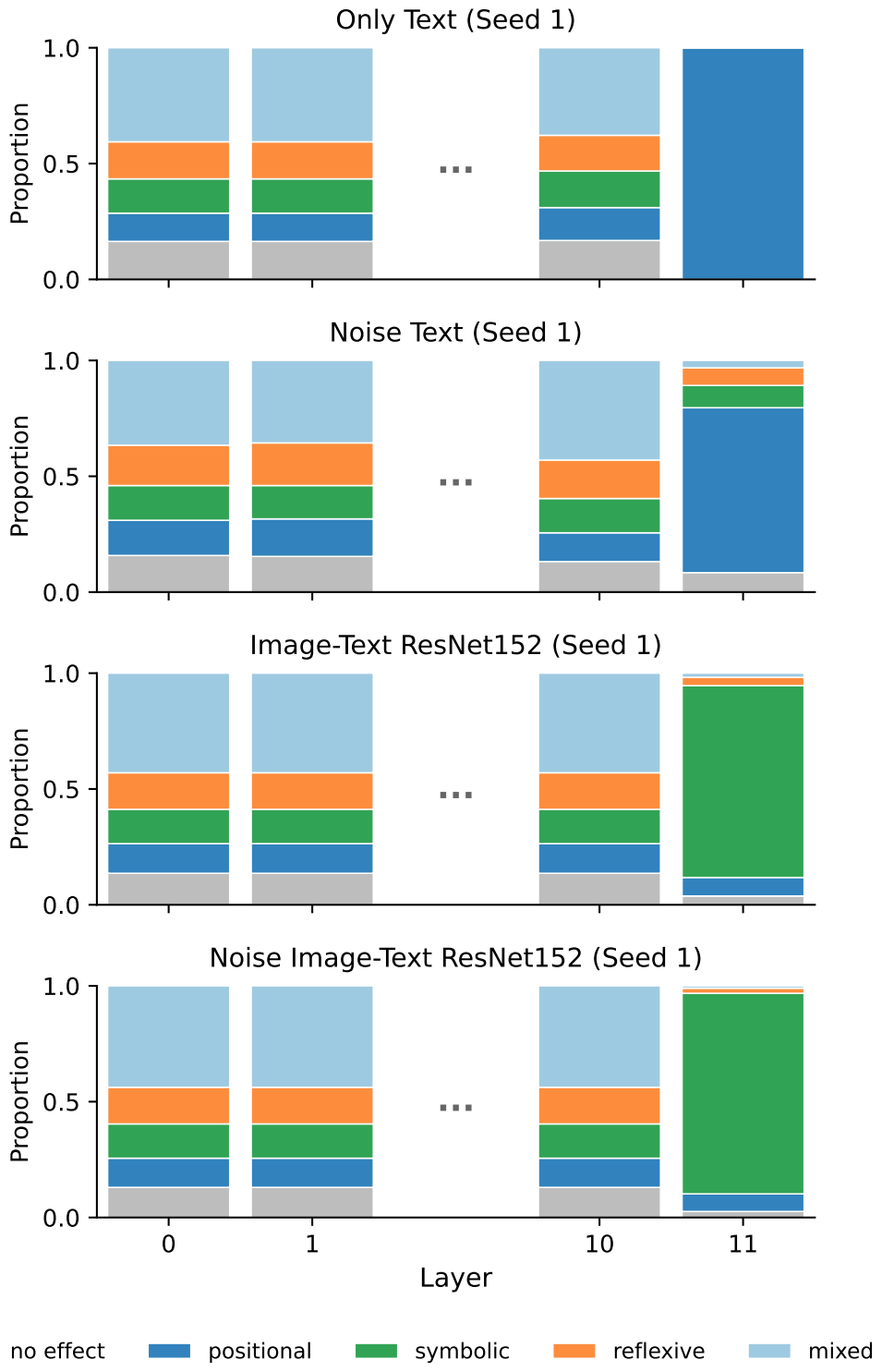

Figure 4: **Binding Mechanism Shift.** Interchange intervention results showing the dominant binding mechanism at each layer across all model variants. Text-only models ($\mathcal{M}_{\text{text-only}}$) rely on the **positional** mechanism (blue). Noise augmentation ($\mathcal{M}_{\text{noise-text}}$) introduces an increase in symbolic binding, but the model remains predominantly positional. Image-trained models ($\mathcal{M}_{\text{image-text}}$ and $\mathcal{M}_{\text{noise-image-text}}$) both transition to a **symbolic** mechanism (orange).

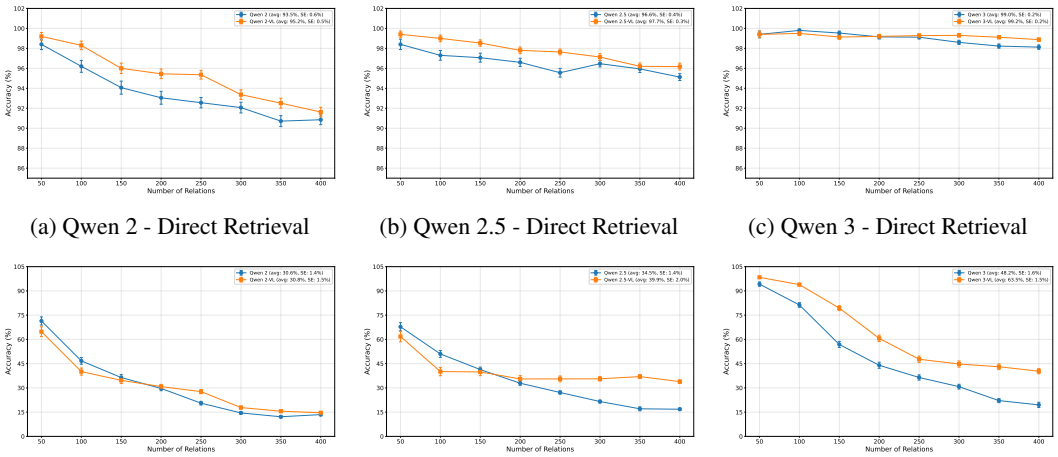

(a) Qwen 2 - Direct Retrieval (b) Qwen 2.5 - Direct Retrieval (c) Qwen 3 - Direct Retrieval

(d) Qwen 2 - Indirect Retrieval (e) Qwen 2.5 - Indirect Retrieval (f) Qwen 3 - Indirect Retrieval

Figure 5: Detailed performance breakdown for all Qwen model generations on the Direct Retrieval and Indirect Retrieval tasks.

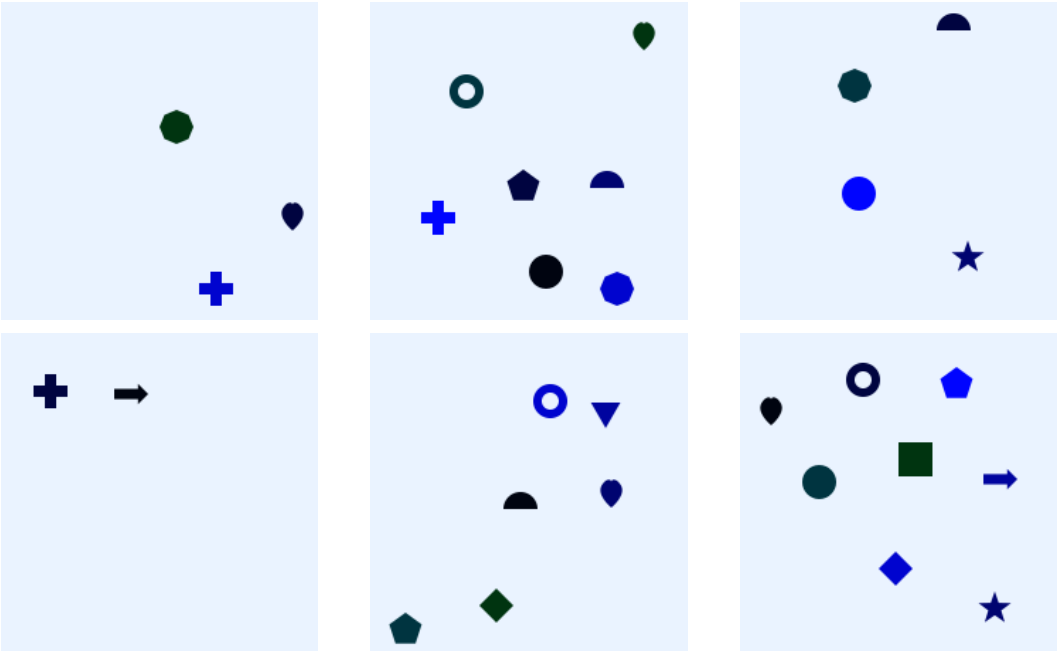

Figure 6: Example rendered contexts for the image modality, showing colored shapes drawn as filled SVG graphics on a white background.

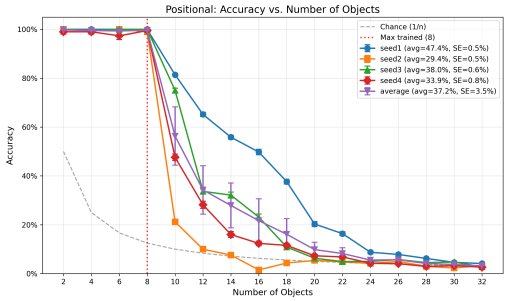

(a) Text-Only ($\mathcal{M}_{\text{text-only}}$)

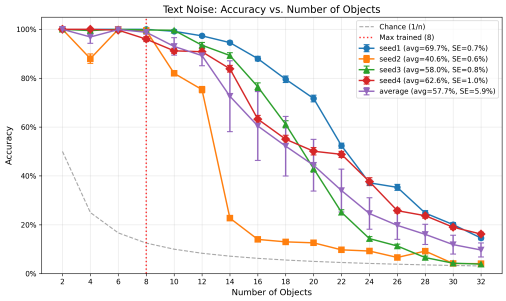

(b) Noise-Text ($\mathcal{M}_{\text{noise-text}}$)

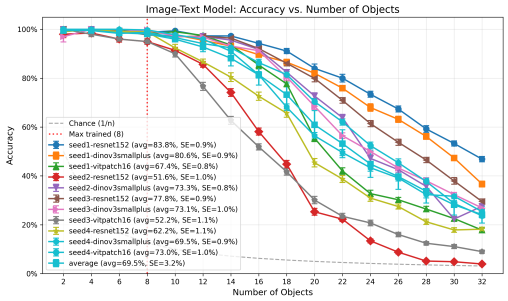

(c) Image-Text ($\mathcal{M}_{\text{image-text}}$)

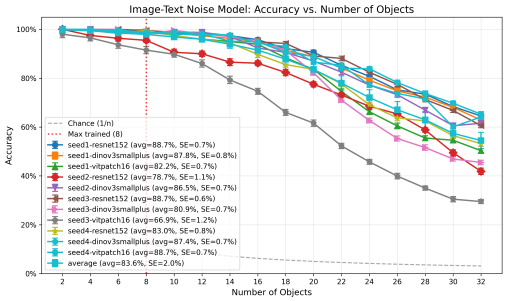

(d) Noise-Image-Text ($\mathcal{M}_{\text{noise-image-text}}$)

Figure 7: Individual generalization plots for the four scratch model variants. The vertical dashed line indicates the maximum sequence length seen during training (8 items).

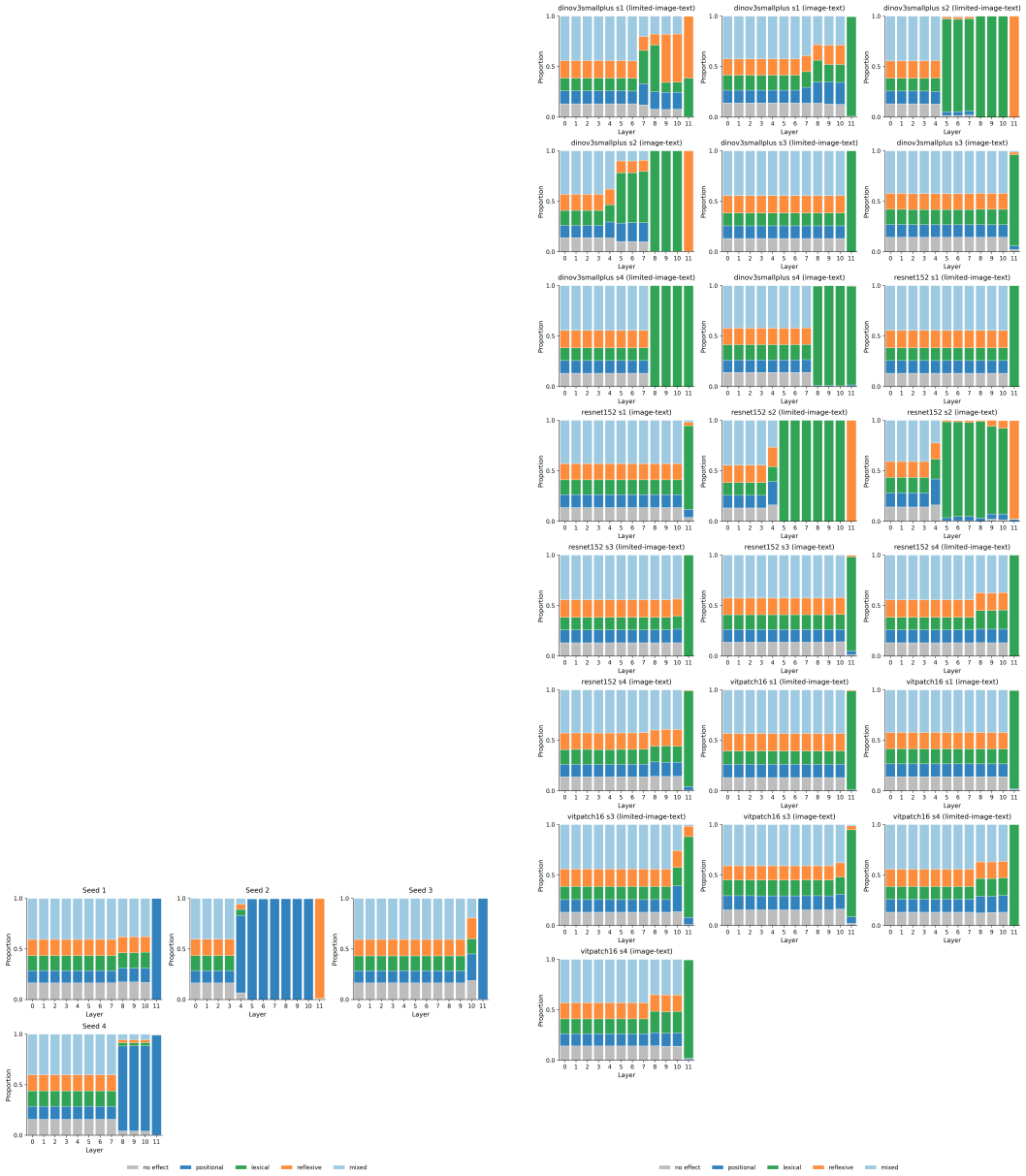

(a) All Text-Only Seeds

(b) All Image-Text Runs

Figure 8: **Aggregate Interchange Results.** (a) Across all 4 random seeds, the text-only models consistently converge to a Positional mechanism, though the specific layer where this mechanism activates varies (e.g., Layer 5 vs Layer 11). (b) Conversely, models exposed to the visual curriculum consistently develop Symbolic binding mechanisms, regardless of the specific image encoder used (ResNet vs ViT vs DINO).

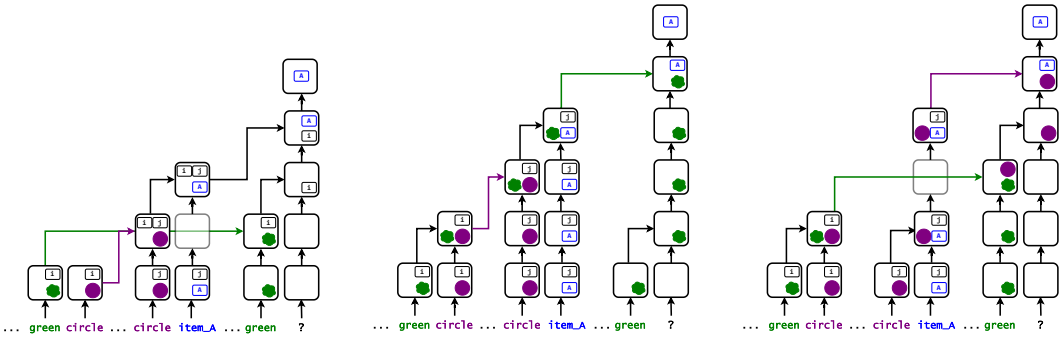

(a) Positional Circuit (b) Symbolic A (Color-Key) (c) Symbolic B (Shape-Key)

Figure 9: **Circuits corresponding to the binding mechanisms.** Early layers encode token-level information (color, shape, item identity). Colored arrows indicate attention-mediated information transfer between tokens. The key distinction: the Positional Circuit transfers only position indices (implicit binding), while Symbolic Circuits transfer semantic content (explicit binding).

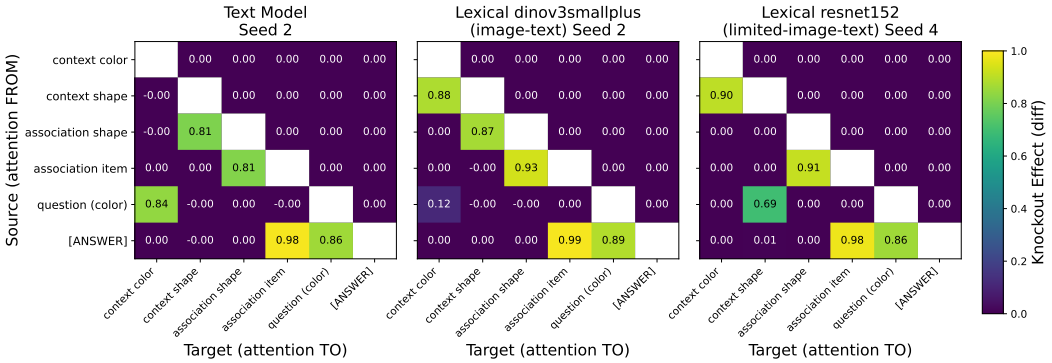

Figure 10: **Attention Knockout Analysis.** Heatmaps showing the drop in performance when attention between specific token pairs is ablated. (a) The Positional mechanism relies on position-matching pathways. (b, c) The Symbolic mechanisms show attribute-routing pathways.

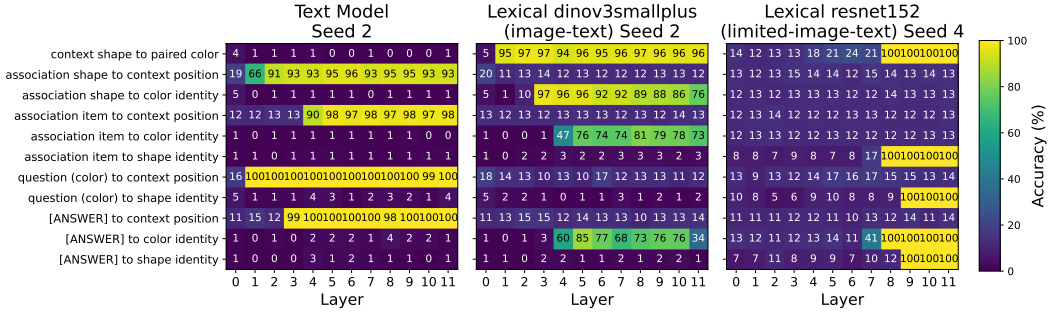

Figure 11: **Linear Probe Analysis.** (a) The Positional model accumulates position but not attribute information at entity tokens. (b, c) Symbolic mechanisms exhibit the "binding signature": attribute decodability surges at entity positions.

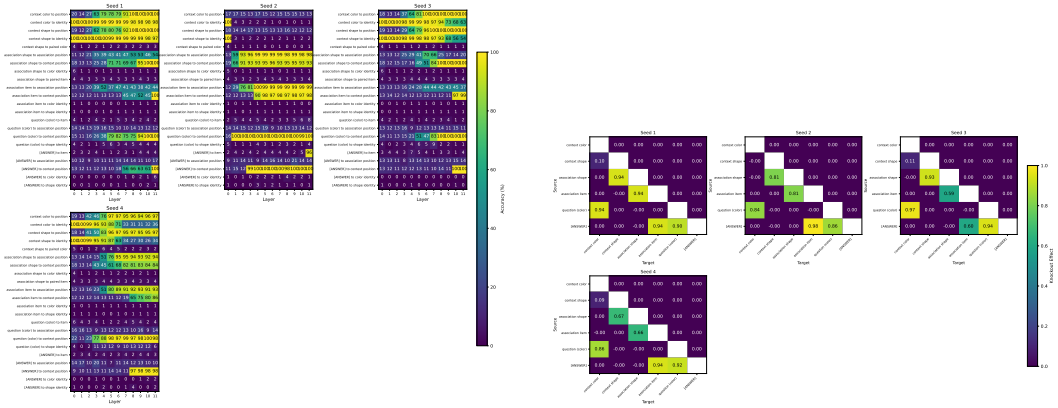

(a) Text-Only - All Seeds (Probes)

(b) Text-Only - All Seeds (Knockouts)

Figure 12: **Aggregate Results: Text Models.** All four seeds show the positional pattern: high position decodability, low attribute decodability at entities, and sparse position-matching knockout matrices.

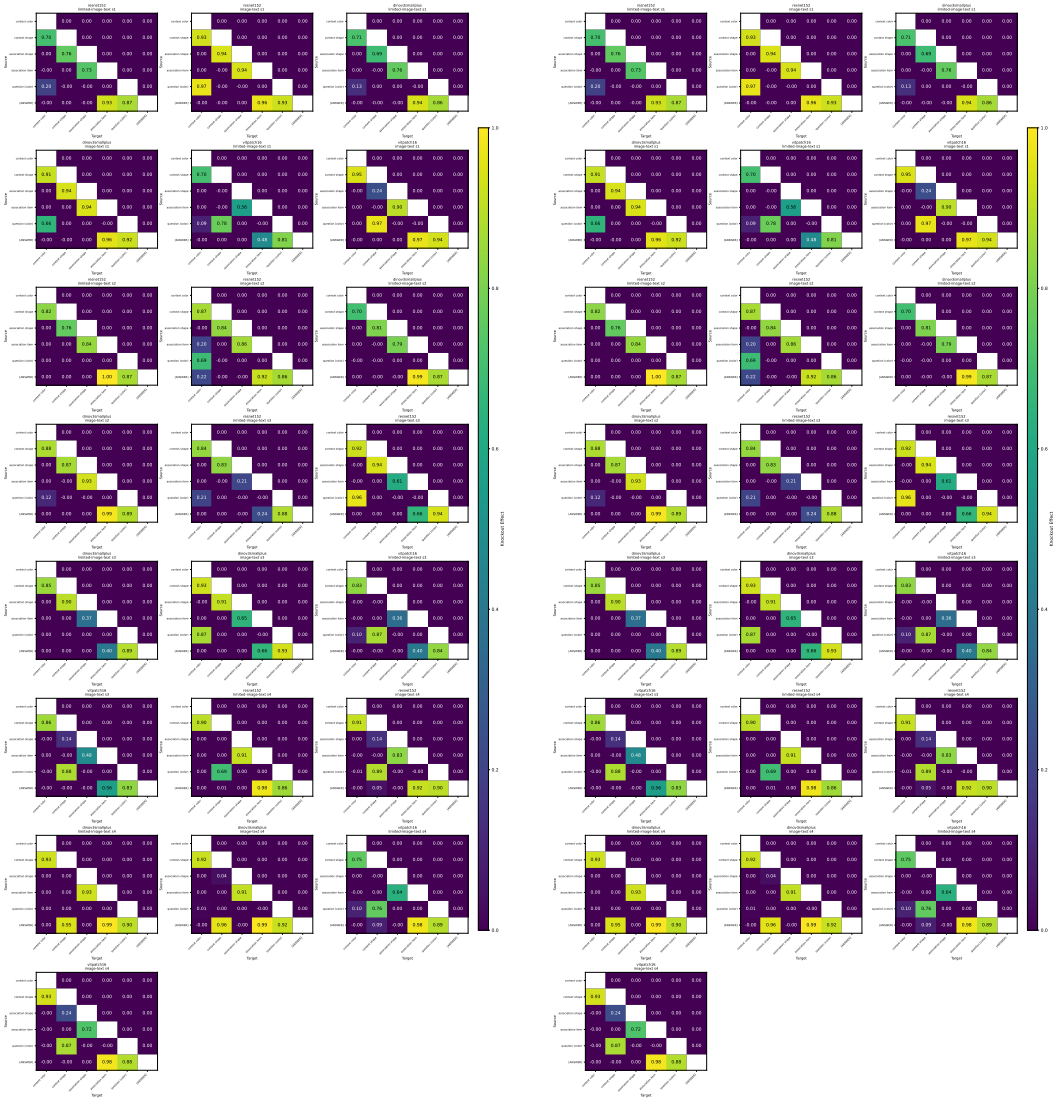

(a) Image-Text - All Runs (Probes)

(b) Image-Text - All Runs (Knockouts)

Figure 13: **Aggregate Results: Image-Text Models.** All twelve runs (4 seeds $\times$ 3 encoders) show the symbolic pattern: binding signature in probes and attribute-routing pathways in knockouts.

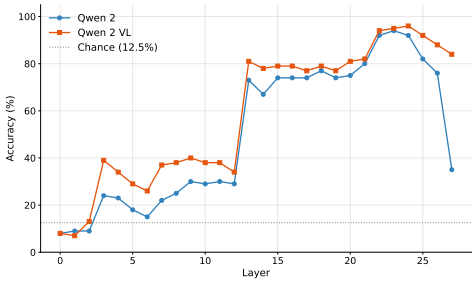

(a) Qwen 2

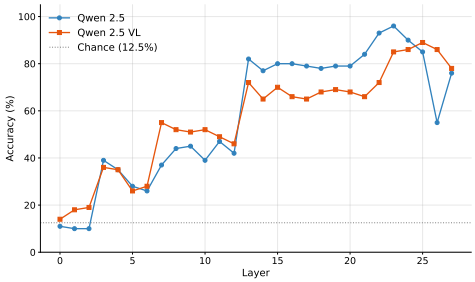

(b) Qwen 2.5

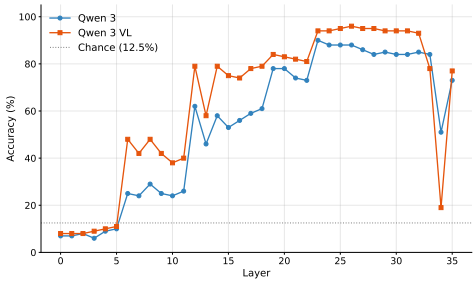

(c) Qwen 3

Figure 14: **Color at Context Shape.** Linear probes decoding color identity at the context shape token position. The VLM models show higher color decodability than their text-only counterparts, indicating binding in context.

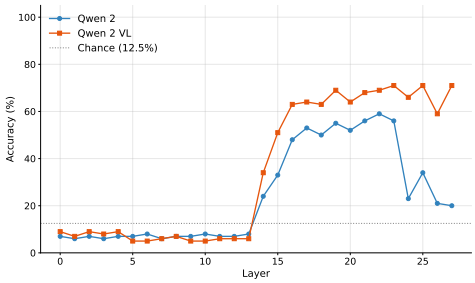

(a) Qwen 2

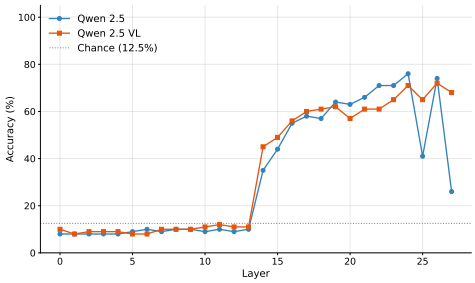

(b) Qwen 2.5

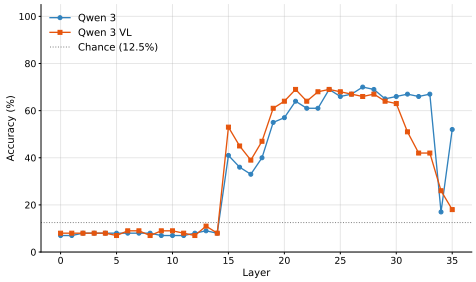

(c) Qwen 3

Figure 15: **Color at Association Shape.** Linear probes decoding color identity at the association shape token position. The VLM models show higher color decodability, consistent with color propagation from context to association.